

**UNIVERSITÉ DU QUÉBEC**

**MÉMOIRE PRÉSENTÉ À  
L'UNIVERSITÉ DU QUÉBEC À CHICOUTIMI  
COMME EXIGENCE PARTIELLE  
DE LA MAÎTRISE EN INGÉNIERIE**

**par**

**YONGMIN CHEN**

**A 2-D RANDOM WALK MODEL FOR PREDICTING ICE  
ACCRETION ON A CYLINDRICAL CONDUCTOR**

**MODÉLISATION EN 2-D DE L'ACCUMULATION DE GLACE  
SUR UN CONDUCTEUR CYLINDRIQUE PAR LA MÉTHODE  
DU CHEMINEMENT ALÉATOIRE**

**Mars 2001**



### Mise en garde/Advice

Afin de rendre accessible au plus grand nombre le résultat des travaux de recherche menés par ses étudiants gradués et dans l'esprit des règles qui régissent le dépôt et la diffusion des mémoires et thèses produits dans cette Institution, **l'Université du Québec à Chicoutimi (UQAC)** est fière de rendre accessible une version complète et gratuite de cette œuvre.

Motivated by a desire to make the results of its graduate students' research accessible to all, and in accordance with the rules governing the acceptance and diffusion of dissertations and theses in this Institution, the **Université du Québec à Chicoutimi (UQAC)** is proud to make a complete version of this work available at no cost to the reader.

L'auteur conserve néanmoins la propriété du droit d'auteur qui protège ce mémoire ou cette thèse. Ni le mémoire ou la thèse ni des extraits substantiels de ceux-ci ne peuvent être imprimés ou autrement reproduits sans son autorisation.

The author retains ownership of the copyright of this dissertation or thesis. Neither the dissertation or thesis, nor substantial extracts from it, may be printed or otherwise reproduced without the author's permission.

## Résumé

Ce mémoire de maîtrise présente un modèle en 2-D qui permet de prédire le profile et le poids de l'accumulation de glace sur un conducteur cylindrique, par la méthode du «cheminant aléatoire», et non pas par l'approche continue classique qui est basée sur la résolution des équations de conservation. Dans cette approche, les gouttelettes sont considérées comme ayant un mouvement aléatoire le long du conducteur ou à la surface de la glace accumulée. Les paramètres du modèle utilisé («cheminant aléatoire»), incluant la probabilité du gel de l'eau, du délestage et du mouvement de celle-ci, sont exprimés en fonction des conditions météorologiques et environnementales. Quelques nouveaux paramètres, notamment les pertes Joule causées par le passage du courant électrique et la direction de la collusion des gouttes d'eau sur le cylindre, sont considérés pour la première fois dans cette approche.

## **Abstract**

This Master's thesis presents a two-dimensional model for predicting the profile and mass of ice accretion on a transmission line conductor, in which the random walk method is used, instead of using the classical continuous approach based on the solution of conservation equations. In this approach, the stochastic motion of fluid elements along the conductor or ice accretion surface is considered. The random walk parameters used in the model, including the freezing probability and the probabilities of shedding and motion, are expressed as functions of the atmospheric conditions. New features of the random walk model, including the heat generated by the electric current and a variable direction of water droplet impingement, are considered for the first time in this approach.

## **Acknowledgments**

This work has been carried out within the framework of NSERC/Hydro-Québec/UQAC industrial chair on Atmospheric Icing of Power Network Equipment (CIGELE), in collaboration with the University of Alberta in Edmonton.

I would like to express my gratitude to my director, Professor M. Farzaneh, for his instructions and support. I am very grateful to my co-director, Professor E. Lozowski in the University of Alberta, for his gentle supervision and encouragement in the project.

I would like to acknowledge Dr. K. Szilder for his valuable advice and help. I express my appreciation to all other professors and members of the CIGELE for their support and help.

Finally, I would like to thank my family and my fiancée for their support and encouragement during my Master's studies.

## Table of Contents

CHAPTER	PAGE
Chapter 1. Introduction . . . . .	1
1.1 Background . . . . .	1
1.2 Objective . . . . .	3
1.3 Methodology . . . . .	4
1.4 Survey of the thesis . . . . .	5
Chapter 2. Review of the literature . . . . .	6
2.1 Analytical models . . . . .	6
2.1.1 Jones simple model . . . . .	6
2.1.2 Chaîné and Castonguay model . . . . .	9
2.1.3 McComber non-circular accretion shape freezing rain model . . . . .	9
2.2 Numerical models . . . . .	12
2.2.1 Time-independent models . . . . .	12
2.2.2 Time-dependent models . . . . .	16
2.3 The Szilder random walk model . . . . .	23
Chapter 3. Model descriptions . . . . .	25
3.1 Two-dimensional morphogenetic model. . . . .	25

3.2 Model modification for considering the Joule heating effect . . . . .	32
3.3 Model modification for considering variable drop	
impingement angles . . . . .	34
Chapter 4. Model simulation results and discussion. . . . .	37
4.1 Model predictions of the ice accretion on a non-energized	
conductor . . . . .	37
4.1.1 Model prediction analyzed as a function of external	
convective heat flux . . . . .	37
4.1.2 Simulation of ice accretion as a function of rainfall rate . . . . .	42
4.2 Model predictions when considering the Joule heating effect . . . . .	45
4.3 Model predictions when considering variable drop	
impingement angles . . . . .	48
4.3.1 Influence of the impinging raindrop angles	
on the ice accretion. . . . .	48
4.3.2 Investigation of the rainfall rate effect on the	
ice accretion under the different impinging raindrop angles . . . . .	56
Chapter 5. Summary and recommendations . . . . .	59
5.1 Summary . . . . .	59
5.2 Recommendations . . . . .	60

References . . . . .	62
Appendix A The FORTRAN program of Makkonen's numerical model . . . . .	65
Appendix B The FORTRAN program of Lozowski's numerical model . . . . .	74

## List of Figures

FIGURE	PAGE
Figure 2.1 McComber rigid cable model accretion shape . . . . .	11
Figure 2.2 Model-predicted accretion profiles of the Lozowski model . . . . .	15
Figure 2.3 Results of the Makkonen model . . . . .	18
Figure 2.4 The time-evolution of the ice load M and the ice deposit diameter D on a 3.5cm diameter wire for the Makkonen model . . . . .	20
Figure 2.5 Sensitivity of ice load M and ice deposit diameter D to variation of the air pressure . . . . .	22
Figure 2.6 Sensitivity of ice load M and ice deposit diameter D to variation of the median volume droplet diameter . . . . .	22
Figure 3.1 Diagram of the raindrop velocity showing the impingement angle $\phi$ . . . . .	36
Figure 4.1 Influence of the convective heat flux on the shape of the ice accretion . . . . .	39
Figure 4.2 Influence of the convective heat flux on the accretion process . . . . .	41
Figure 4.3 Influence of freezing rainfall rate on the ice accretion characteristics . . . . .	43
Figure 4.4 Influence of the external convective heat flux on the ice accretion under simulations without and with the Joule heating effect . . . . .	46

Figure 4.5 Influence of the convective heat flux on the accretion process for varying raindrop impingement angles . . . . .	49
Figure 4.6 Ice accretion shape development with increasing external heat flux under a 30° raindrop impingement angle . . . . .	51
Figure 4.7 Influence of the median volume droplet impingement angle on the ice accretion characteristics . . . . .	53
Figure 4.8 Accretion shapes for simulations with various impingement angles. . . . .	55
Figure 4.9 Influence of rainfall rate on the ice accretion for two “typical” impingement angles . . . . .	57

## CHAPTER 1

### INTRODUCTION

#### 1.1 Background

In Canada as in many other cold countries, ice accumulation due to freezing rain, freezing drizzle, in-cloud icing, icing fog, and wet snow may cause significant damage to power network equipment and significantly reduce its reliability. Usually, the occurrence of icing is accompanied by wind. Ice storms caused by freezing rain and freezing drizzle may have the most severe effect (Environment Canada, <http://www.msc-smc.ec.gc.ca/events/icestorm98>). Freezing rain occurs with the temperature of falling raindrops near the freezing point and the air temperature below the freezing point. It may coat every exposed surface with a thick layer of ice. The ice weight coupled with wind loading effects (including galloping) may result in the breakage of power lines, ground wires and insulators, and the collapse of their supporting structures (towers and poles). Such storms are almost yearly events in Canada and their social and economic impact may be enormous.

In the great ice storm of January 1998 in Eastern Canada and the North-eastern United States, prolonged freezing rain brought down 120,000 km of power lines and telephone cables, 1,300 major transmission towers each worth about \$100,000 and about 27,000 wooden utility poles costing about \$3,000 each. 1,500,000 households in Canada were without power. The damage in Eastern Ontario and Southern Quebec was so severe

that major rebuilding, not merely repairing, of the electrical grid had to be undertaken. What took human beings a half century to construct took nature a matter of days to knock down. Storm-related costs are estimated to be close to two billion dollars (Environment Canada, <http://www.msc-smc.ec.gc.ca/events/icestorm98>).

Mitigating the effects of ice storms is not easy. Dimensioning the structures to endure heavier ice loads rapidly increases the construction costs. Consequently, in order to optimize the design of power transmission line structures, it is very important to have estimates of the intensity of icing under a range of conditions and of the extreme ice loads.

Such estimates can be obtained by collecting long time series of observations on ice loads. The use of icing data for this purpose has been possible to some extent in parts of the former USSR (Nikiforov, 1983), where observations of ice accretion on cables have been included in routine meteorological observations. However, in other countries, such an approach has been found to be too time-consuming and laborious for the purpose of planning power lines.

An alternative approach is to use theoretical modelling. This kind of modelling takes into account the basic physical processes that control the rate of icing on wires. In this approach, general relationships can be derived between the intensity of icing and meteorological parameters, for power line structures of various sizes and orientations. Using historical meteorological data along with icing models, extreme ice loads can be predicted and can be used to draw up reliable regional power line structural design criteria.

## 1.2 Objective

Classical numerical models, which are based on differential forms of the equations for the conservation of momentum, energy and mass, have been used to predict ice accretion shapes and loads. Such models are called continuous, since they are based on the assumption of continuous changes of all the physical parameters. Such models have the shortcoming that they cannot simulate the complexity of the ice structure. This complexity leads to a number of important physical effects which may tend to increase the ice load.

Instead of using the continuous approach, a hybrid analytical and random-walk model that includes empirically based freezing probability and shedding parameters was presented by Szilder (1994). The random walk model (also called a morphogenetic model) builds up an ice accretion structure using discrete elements or particles. Each particle could be a drop or drop ensembles. After its contact with the existing ice accretion, it can move along the surface of the ice accretion before freezing. The particle mobility is formulated in the model using a Monte Carlo approach. The model parameters that control the surface motion and the freezing of the particles are functions of atmospheric conditions. Such a model allows the efficient representation of water flow along the accretion surface, since the fluid elements can move considerably away from the location of their initial impact. The random walk model also adds some stochastic variability to accretion shapes in keeping with the experimental observations.

The objective of the current work is to create a two-dimensional, random walk model which predicts the shape and mass of ice accretions on a transmission line conductor, under a variable direction of water droplet impingement, and allowing for Joule

heating due to current flow in the conductor. We choose a two-dimensional rather than a three-dimensional model, because the two-dimensional model has a smaller requirement for computing time and memory, and it also has the advantage of more convenient visualization.

Previously published random walk models supposed the impinging drops to fall vertically. Hence the effect of a variable impingement direction for the water droplets has not so far been investigated and published. For icing on a transmission line conductor, the effect of Joule heating is also important in order to predict accurately both the accretion shape and the mass of the ice deposit. In the current investigation, both the Joule heating effect of the electric current and a variable direction of impinging raindrops will be considered (as one would expect for freezing rain under a range of wind speeds).

### 1.3 Methodology

The main method used in the research is two-dimensional numerical modelling. Based on the theoretical model, a numerical model can be realised by using computer programming. The two-dimensional model has less computing time consumption and has the advantage of more convenient visualisation. The computer language used in the programming is Fortran 77. This model can make predictions of the mass and profile of the ice accretion on wires, either in data sets or in computer plots. All the parameters in the model can be analysed by changing the input data to the program, and the model can be modified easily to add new features.

#### 1.4 Survey of the thesis

In Chapter 2, a review of previous freezing rain models applicable to transmission lines is presented. In Chapter 3, a two-dimensional random walk model will be introduced, and the main modifications necessary for the current investigation will be explained. In Chapter 4, the simulation results and a discussion of them will be presented. Conclusions and recommendations for further investigation will be included in Chapter 5.

## CHAPTER 2

### REVIEW OF THE LITERATURE

Attempts to theoretically estimate glaze ice loads applicable to transmission line icing based on meteorological data have been made for over 50 years. There are various models used operationally and in theoretical studies today. Different modelling approaches are taken. Some analytical models have focused on the effect of an average freezing rain intensity on a simplified shape, which in the majority of cases is a circular cylindrical accretion shape, while detailed numerical models simulate the formation of the accretion shape based on detailed drop trajectories and heat transfer, expressed as conservation of momentum, energy and mass equations under specified boundary and initial conditions.

#### 2.1 Analytical models

The analytical approach consists in making a simple accretion shape assumption a priori. The simple freezing rain model of Jones (1996) is typical of this approach.

##### 2.1.1 Jones simple model

The model first takes a simple approach by considering rain falling with no wind, and vertical raindrop trajectories perpendicular to a horizontal flat plate. If the weather is cold enough, the water does not pool or run off; instead the rainwater freezes to form a uniform layer of ice that is uniformly thick on the plate no matter what its size. If the density  $\rho_i$  of this ice is  $0.9 \text{ g/cm}^3$ , a 1 cm rainfall results in a uniform 1.1 cm thick ice layer.

This concept can now be extended to cylinders. We consider long circular cylinders of various diameters suspended horizontally above the ground in the same windless rainstorm. The 1 cm of freezing rain also falls on each of these cylinders. If all the impinging water freezes in a uniform radial accretion, then this centimeter of rainfall is spread uniformly as ice over the surface of the cylinders. Because the perimeter is a factor of  $\pi$  larger than the cylinder diameter, the uniform radial ice thickness  $R_{eq}$  on each horizontal cylinder is:

$$R_{eq} = \frac{\rho_w}{\rho_i} \frac{1}{\pi} = 0.35cm \quad (2.1)$$

where  $\rho_w = 1.0g/cm^3$  is the density of water. As long as the ice accretes uniformly around the cylinder, the cylinder cross sections remain circular. Therefore, the ratio of the diameter of each iced cylinder to the perimeter of its cross section remains  $1/\pi$  throughout the freezing rain storm, and the ice thickness on the cylinders is independent of their diameters.

Typically, since there is wind during freezing rain storms, the horizontal flux of wind-blown rain must be included in this simple model. Best (1949) related liquid water content to precipitation rate:

$$w = 0.067P^{0.846} \quad (2.2)$$

where  $P$  is the precipitation rate in mm/hr and  $w$  is the liquid water content of the rain-filled air in  $g/m^3$ . Then assuming that all raindrops are moving horizontally at the wind speed, the horizontal flux of water is  $Vw$  ( $g/m^2s$ ) or  $0.36Vw$  ( $g/cm^2hr$ ), where  $V$  is the wind speed in m/s. The total water flux  $W$  is obtained by converting to a consistent set of units and adding vectorally the horizontal flux of wind-blown rain to the vertical flux  $P\rho_w/10$  ( $g/cm^2hr$ ) of falling rain:

$$W = \left[ (0.1P\rho_w)^2 + (0.36Vw)^2 \right]^{1/2} g/cm^2 hr \quad (2.3)$$

The uniform radial ice thickness on a circular cylinder (also called the radial equivalent ice thickness) is then:

$$R_{eq} = \frac{N}{\rho_i \pi} \left[ (0.1P\rho_w)^2 + (0.36Vw)^2 \right]^{1/2} cm \quad (2.4)$$

where  $N$  is the number of hours of freezing rain with precipitation rate  $P$  (mm/hr) and wind speed  $V$  (m/s).

During a storm, the precipitation rate and wind speed, which vary in time, are typically measured hourly at weather stations, so Equation (2.4) can be written more generally as:

$$R_{eq} = \frac{1}{\rho_i \pi} \sum_{j=1}^N \left[ (0.1P_j\rho_w)^2 + (0.36V_j w_j)^2 \right]^{1/2} cm \quad (2.5)$$

where  $P_j$ ,  $w_j$  and  $V_j$  are the average precipitation rate, liquid water content and wind speed in the  $j$ th hour of a storm lasting  $N$  hours. This equation shows that the uniform radial ice thickness in the simple model is independent of cylinder diameter and depends only on two meteorological parameters: precipitation rate and wind speed.

This simple ice accretion model for horizontal circular cylinders is based on three principal assumptions: first, the collision efficiency of the rain drops with the cylinder is 1. For freezing rain, the mode of the drop diameter distribution is typically around 1 millimeter. Considering the size of typical conductors and typical wind speeds, the collection efficiency is expected to be 1.0 practically. Secondly, all the rain impinging on

the cylinder freezes, and so there is no shedding. In other words, the growth mode is dry. This does not mean that there is no liquid flow along the surface, only that there is no shedding or splashing. And thirdly, the ice accretes uniformly around the circumference of the cylinder, so the formation of icicles and asymmetrical shapes is ignored.

### 2.1.2 Chaîné and Castonguay model

Chaîné and Castonguay (1974) developed one of the first analytical models for transmission lines. Instead of assuming a circular accretion shape, their model assumes a semi-elliptical accretion shape on one side of the cable. They then define a correction factor  $K$  which they determined empirically from the marine icing wind-tunnel experiments of Stallabrass and Hearty (1967). They defined  $K$  to be the ratio of the actual cross-sectional area of the accretion to the one calculated using their semi-elliptical assumption. Since the shape correction factor  $K$  is determined by the experimental data to be a function of cable radius  $R_0$  and air temperature, the Chaîne model results show a strong dependence of radial equivalent ice thickness on cable diameter.

### 2.1.3 McComber non-circular accretion shape freezing rain model

A circular, cylindrical accretion shape is assumed in many freezing rain models. This type of shape is observed with torsionally flexible cables or conductors, but non-circular shapes form on more rigid conductors. The ice shape hypothesis influences the icing rate chiefly through its rain collecting cross-section. This becomes significant for long events and can lead to important differences in load estimation. In order to investigate how

significantly the shape hypothesis can affect the computed maximum ice loads, McComber (2000) presented a model with a non-circular shape assumption more realistic for torsionally stiff conductors.

The evolution of the ice accretion shape depends on its orientation with respect to the direction of the impinging drops. Depending on its torsional flexibility, the iced cable will twist when the eccentric ice shape creates a torque. Hence, a more circular shape develops for more flexible cable spans. The torsional flexibility of cables is considerably different for a very flexible ground wire and for a fairly stiff sub-span bundled conductor. Without adequate field measurements, the accurate estimation of the flexibility of a stranded transmission line cable or conductor is almost impossible. Considering this lack of field measurements, McComber proposed that icing models could rely on an approximation based on a combination of two extreme cases: a very flexible and a very rigid cable. He then proposed that through the use of a rigidity factor, an adjusted modelling result for a cable with a specific torsional stiffness could be obtained.

Assuming a rigidity factor,  $f_k$ , lying between the value 1 for a rigid cable and 0 for a flexible cable, the radial equivalent thickness,  $R_{eq}^m$  for a cable with a known rigidity can be estimated as a weighed average of the flexible cable radial equivalent thickness,  $R_{eq}^f$  and the rigid cable radial equivalent thickness,  $R_{eq}^r$ .

$$R_{eq}^m = f_k R_{eq}^r + (1 - f_k) R_{eq}^f \quad (2.6)$$

For the flexible cable case, a circular accretion shape is assumed. For this case, McComber used the same approach as the Jones simple model. Taking into account the fact that the dry growth accretion shape on a fixed conductor is the result of the range of drop impingement

angles and allowing for spread of water on impact when the water runs back before freezing, a simple accretion shape assumption for a stiff cable has been suggested by McComber. As described in Figure (2.1), a linear variation of thickness is distributed over three quarters of the conductor's perimeter. The mass is assumed arbitrarily to be equally divided on both sides of the average drop incident direction  $\phi$ .

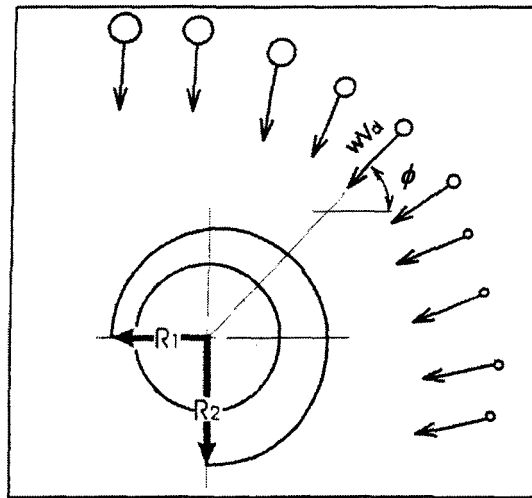


FIG. 2.1 McComber rigid cable model accretion shape

Hence in the absence of wind, there will be more mass on top of the cable, and if wind is strong, mass will be added on the side. This shape is the basis of a stiff or rigid cable model. The two parameters,  $R_1$  and  $R_2$ , describing the shape are computed from the geometry shown in Figure (2.1). The volume increment is  $R_{eq}$  calculated using Equation (2.4), multiplied by  $\pi$  and the accretion cross-section,  $D_i$ .

If a rapid approximation of radial ice thickness is required, the ice shape can be simplified further by assuming a uniform thickness extending over three quadrants of the

cable perimeter (ie.  $R_1 = R_2$ ). In this case, the right-hand-side of Equation (2.4) is divided by 0.75.

In order to illustrate the influence on the prediction of the ice load of this accretion shape, McComber compared the radial equivalent thickness and ice loads obtained on a typical conductor using the different models and the meteorological data of the January 1998 Ice Storm. The rigid cable model yields a significant increase of 27.3% in the maximum ice loads for a transmission line normal to the prevailing winds, when compared with the more widely used circular ice shape model.

## 2.2 Numerical models

The primary advantage of numerical modelling is that time-dependent effects can be incorporated and, therefore, also temporal changes in the input (environmental conditions) parameters can be easily taken into account. Moreover, they can also simulate rime icing (dry growth) and the models can detect the growth mode by heat balance calculations. Thus, these models need no pre-assumptions about the icing mode or the ice shape. Two main categories of continuous numerical models can be distinguished: time-independent and time-dependent.

### 2.2.1 Time-independent models

In time-independent models (e.g. Lozowski et al., 1983), the ice-shape calculations are based on the assumption that the initial growth rate remains unchanged during the

simulation. Such models are therefore most appropriate for simulating short icing episodes (for example, in aircraft icing).

In 1983, Lozowski and others introduced a time-independent model which simulates icing on an unheated, non-rotating cylinder. Both rime and glaze ice can be accounted for in the model. The model computes the thermodynamic conditions and the initial icing rate as a function of angle around the upstream face of the cylinder.

The situation under consideration in the model is one in which an unheated, non-rotating cylinder of diameter  $D_c$  is located in a uniform airstream of velocity  $U$  far upstream of the cylinder. The airstream contains a cloud of super-cooled water droplets, with a certain size spectrum and liquid water content  $w$ . The droplets are assumed to possess the air temperature  $t_a$  and to move with velocity  $U$  far upstream of the cylinder.

The formulation of the model consists of three parts: first, the local impingement flux of super-cooled water is computed as a function of position around the upstream surface of the cylinder. Second, the steady-state heat balance equation is solved, again as a function of position, in order to determine the local surface temperature and the initial rate of ice accumulation. Finally, the rate of ice accumulation is used to forecast the local ice growth rate and thus the local thickness of ice after a specified time interval. By plotting these thicknesses around the cylinder, the accretion shape and its cross-sectional area or mass can be determined.

In determining the local rate of droplet impingement, the upwind face of the cylinder was divided into 19 angular sectors, each  $5^\circ$  in width and centred on the angles  $5i^\circ$  ( $i$  from 0 to 18). The droplet size spectrum is also discretized by dividing it into nine

diameter categories, each  $5\mu\text{m}$  wide and centred on diameters  $D_j = 5j \mu\text{m}$ , ( $j$  from 1 to 9). For each angular and droplet size category, the local collision efficiency is calculated, and the overall collision efficiency for each sector is the mass-weighted mean for all the droplet size categories. Using this collision efficiency, the liquid water mass flux impinging on each sector can be calculated. The liquid water mass flux is then used to evaluate the terms in the steady-state heat balance equation, which describes the thermodynamics of the accretion. The freezing fraction can be obtained from the heat balance equation. From this freezing fraction, the runback flux can be calculated, and, consequently, the icing flux for each sector can be obtained. Finally, the local thickness after a specified accretion time can be calculated and, by plotting the thickness as a function of angle and interpolating the points, a smooth profile shape of the accretion can be determined.

The present author wrote a Fortran code based on this numerical model (the original code was written in BASIC). The program was written in the Fortran 77 language and compiled using a Fortran 77 compiler running under the IRIX system on an SGI workstation. The program is listed in Appendix B.

Model-predicted accretion profiles for a number of cases in the original paper, which typify the range of profile types, are presented in Figure (2.2). Although the model may be applied quite generally, the model results presented here are applicable to typical aircraft icing conditions.

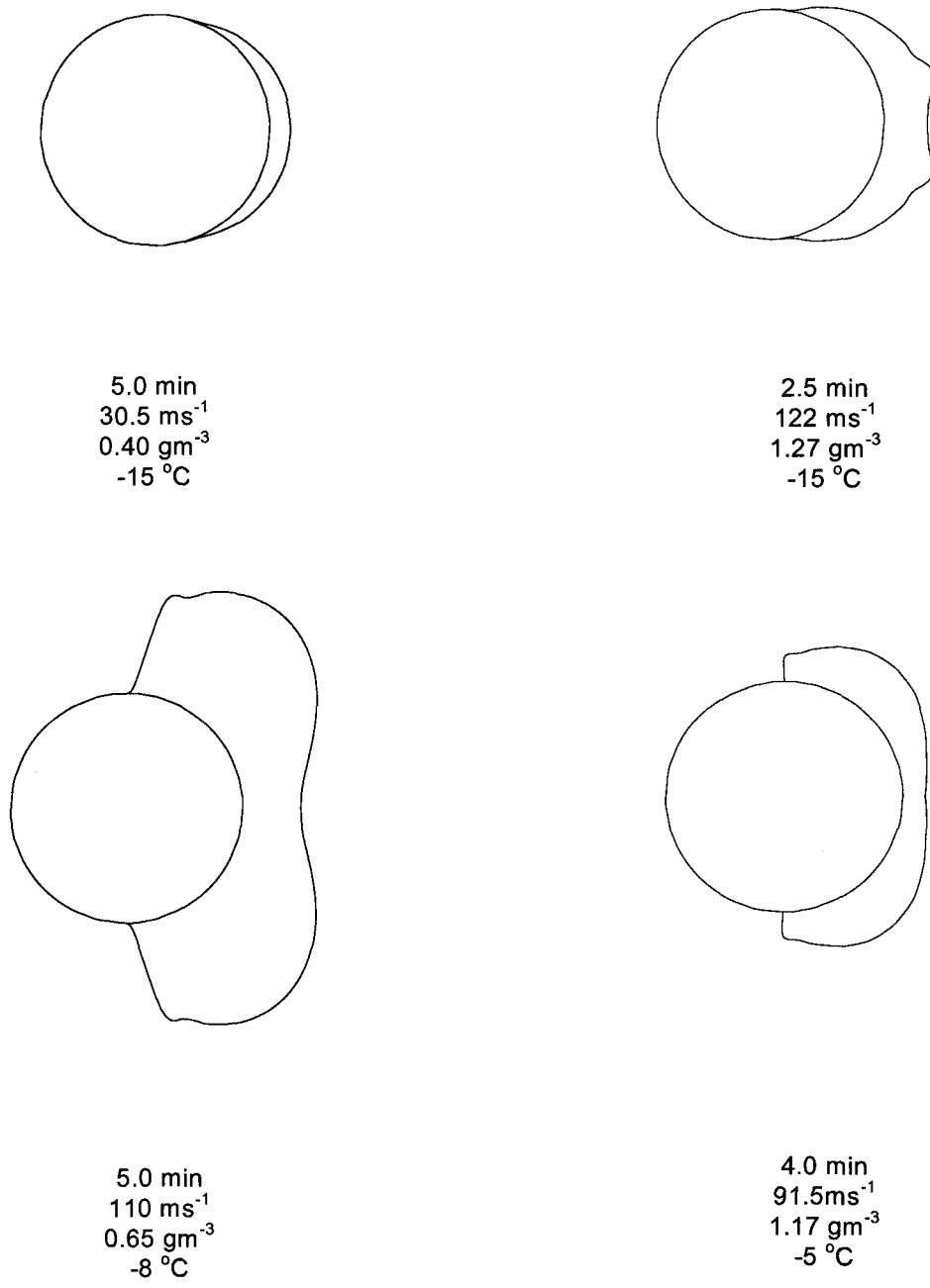


FIG. 2.2. Model-predicted accretion profiles, under the specified conditions of ambient air temperature (°C), airspeed (ms<sup>-1</sup>), cloud liquid water content (gm<sup>-3</sup>) and accretion time (min).

### 2.2.2 Time-dependent models

Time-dependent models try to take into account, to varying degrees, the fact that the growing accretion changes the fluid flow around the object, the trajectories of the incoming droplets and the heat-transfer conditions (e.g. Makkonen, 1984; Baker et al., 1986; Szilder et al., 1987).

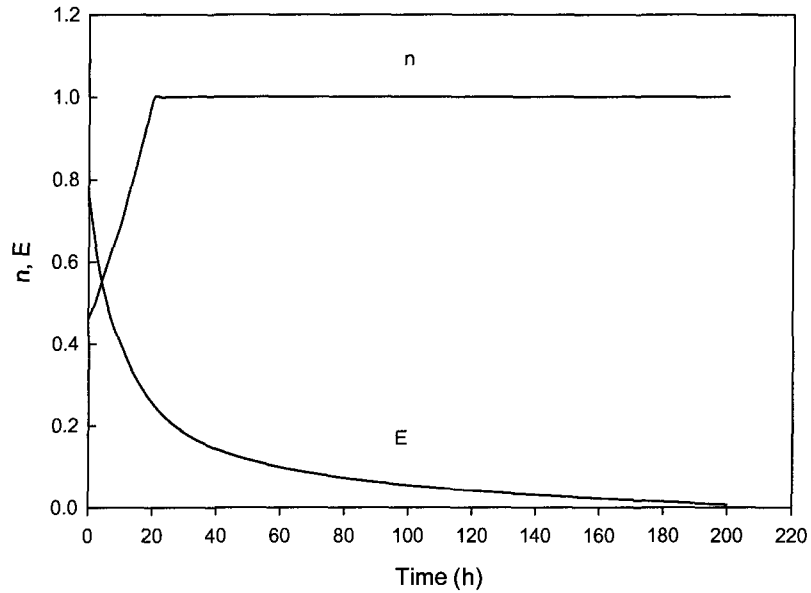
In 1984, Makkonen presented a time-dependent numerical model which is particularly suitable for the simulation of wire icing. The model assumes that the ice accretion maintains a cylindrical profile. The changes in the rate of ice accretion due to the increase of the ice deposit size, as well as the variation of ice density are computed in the model. The model simulates the accretion of super-cooled water droplets onto a wire such as an overhead conductor. A wind direction perpendicular to the wire is assumed. Initially, the water droplets are assumed to move horizontally in the airstream during foggy or in-cloud icing conditions. Ice accretion in freezing rain at low wind speeds and snow accretion were not considered, because modelling of wet snow accretion involves the snow content of air and the aerodynamics of snowflakes, both of which are poorly known. Freezing rain during low wind speeds may involve icicle formation. A subsequent model by Makkonen (Makkonen, 1988) has incorporated icicle formation effects into the original model.

In Makkonen's model, the calculation of the ice load,  $M$ , is made in a stepwise manner. For each time step, the ice load  $M$  is calculated as a function of the icing intensity, (the rate of increase in the mass of ice divided by cross-sectional area of the part of the surface of the ice deposit that faces the wind),  $I$ , the ice deposit diameter  $D$ , the collection efficiency  $E$ , freezing fraction  $n$ . The density of the accreting ice,  $\rho$ , and the mean density

of the total ice deposit,  $\bar{\rho}$ , are calculated as output parameters. During the process of ice accretion on a structure, the dimensions of the ice deposit change. In this model, this effect is restricted to an increase in the ice deposit diameter  $D$ . The icing intensity,  $I$ , is the product of the collection efficiency  $E$ , freezing fraction  $n$ , the wind speed  $v$  and the liquid water content in the air  $w$ . The collection efficiency,  $E$ , is calculated based on the median volume diameter of the droplet distribution. The freezing fraction,  $n$ , is calculated from the heat balance of the icing surface. The ice load,  $M$ , is calculated as a function of icing intensity and the ice deposit diameter at the end of the previous time step. The density of the accreting ice,  $\rho$ , is also calculated as a function of the median volume droplet diameter, the mean surface temperature of the ice deposit and the impact speed of the droplets at the stagnation region. With the ice load and density of the accreted ice, a new ice deposit diameter,  $D$ , can be calculated for each time step. The mean density of the total ice deposit,  $\bar{\rho}$ , for each time step, is obtained from the ice load and the ice deposit diameter. All of the parameters calculated in a particular time step are provided as input parameters for the next time step.

A Fortran program was written by the present author to perform the numerical calculations for Makkonen's ice accretion model. The program was written in the Fortran 77 language, and compiled under the Unix system. A Silicon Graphics workstation was used to code and debug the program. The program is listed in Appendix A.

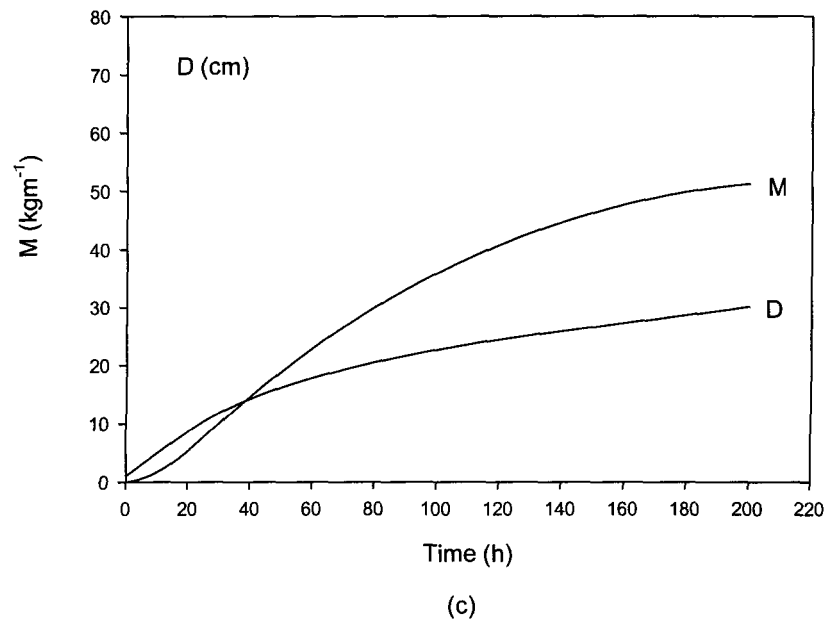
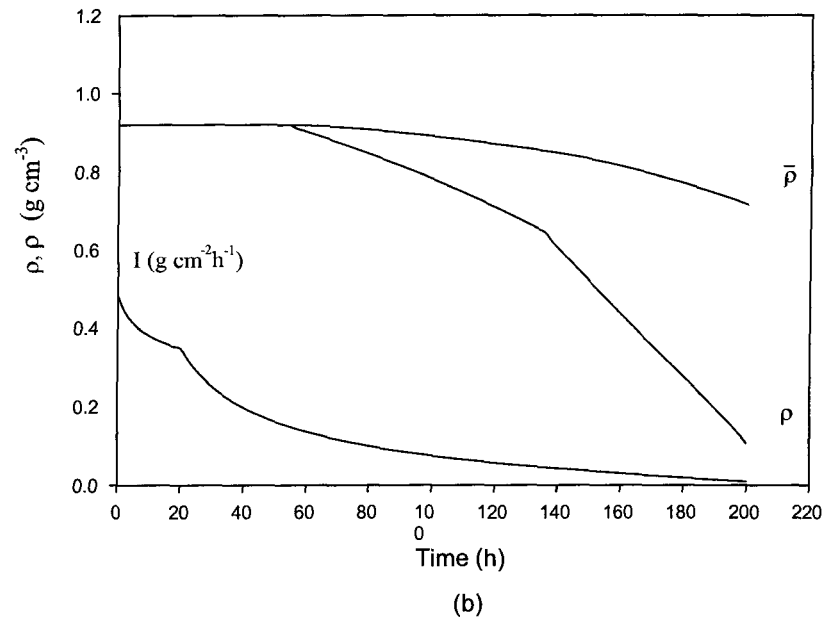
Using the same parameters as in Makkonen's paper, we ran the program to get the results shown in Figure (2.3 a, b, c), which correspond very well with Figs 2 and 3 in the original paper. These validate the essential correctness of the Fortran program coding.



(a)

FIG. 2.3. Some results of the Makkonen model. Wind speed  $20\text{ms}^{-1}$ , air temperature  $-1^{\circ}\text{C}$ , wire diameter 1 cm, cloud liquid water content  $0.3\text{gm}^{-3}$ , and median volume droplet diameter  $25\mu\text{m}$ . (a) Time-evolution of the freezing fraction  $n$  and the collection efficiency  $E$ . (b) Time-evolution of the density of accreting ice  $\rho$  and the total deposit density  $\bar{\rho}$  and the icing intensity  $I$ . (c) Time-evolution of the ice load  $M$  and the ice deposit diameter  $D$ .

Input parameters typical of rather severe atmospheric icing were used in the simulation. As shown in the figures, the model demonstrates that the growth rate of the ice load first increases and then decreases with time in the dry growth regime (rime). The growth regime may change from wet growth (glaze) to dry growth (rime) even under constant atmospheric conditions. The density of the accreted ice decreases with time once dry growth conditions have been reached. This affects the growth rate of the ice load. The relationship between the accreted ice load and the prevailing atmospheric conditions depends strongly on the duration of the icing process.



Other simulation results from Makkonen's model show that decreasing air temperature may lead to either increasing or decreasing ice loads depending on the other atmospheric parameters and on the icing duration. Ice load, particularly in long-term icing, is very sensitive to the median volume droplet diameter in the icing fog or cloud.

The Makkonen program was used in the calculation of the ice load under "typical" transmission line icing rime conditions: wire diameter 35mm, wind speed  $10 \text{ ms}^{-1}$ , air temperature  $-10^\circ\text{C}$ , relative humidity 90%, median volume droplet diameter  $25\mu\text{m}$ , liquid water content  $0.3\text{gm}^{-3}$ . The accretion duration was 24 hours and the time step was 10 minutes. Figure (2.4) shows the time-evolution of the ice load,  $M$ , and the ice deposit diameter  $D$  for this case.

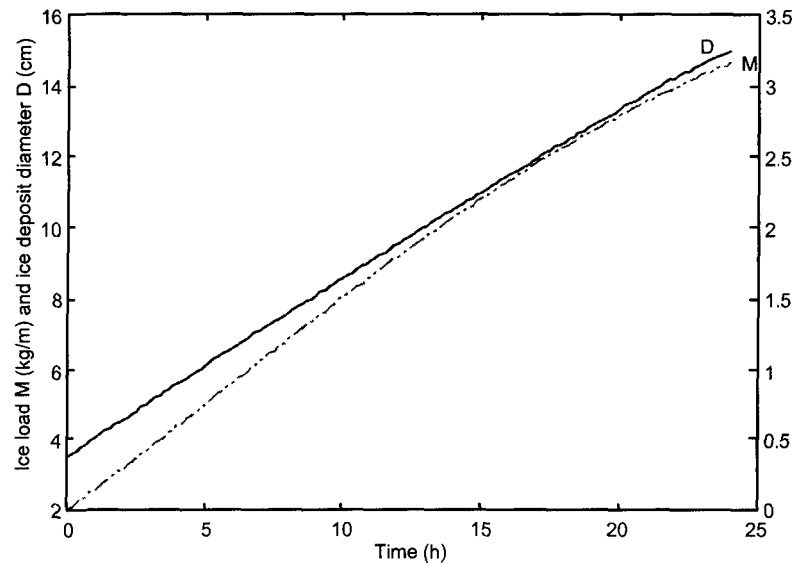


FIG. 2.4. The time-evolution of the ice load  $M$  and the ice deposit diameter  $D$  on a 3.5cm diameter wire. The wind speed is  $10 \text{ ms}^{-1}$ , air temperature  $-10^\circ\text{C}$ , relative humidity 90%, liquid water content  $0.3\text{gm}^{-3}$  and median volume droplet diameter  $25\mu\text{m}$ .

Since under such condition, the entire accretion is in the dry growth regime, the ice deposit diameter and the ice load both increase monotonically (but not linearly) with time.

Air pressure is inversely related to the height of the ice accretion site, so it is an important parameter in ice accretion prediction, because some transmission lines pass through high altitude regions. We used Makkonen's model to test the effect of the air pressure on the ice accretion. The sensitivity of the ice load and the ice deposit diameter to the variation of air pressure, under the same conditions as in Figure (2.4), is shown in Figure (2.5). As the air pressure increases from 70KPa to 100KPa, the ice load and the ice deposit diameter decrease by 13% and 2% respectively. This occurs in part because, in Makkonen's model, the collection efficiency decreases with an increase in air pressure. Also the density of the ice deposit decreases more slowly when the growth regime changes from wet growth to dry growth at low air pressure. Consequently the ice load decreases faster than the ice deposit diameter as the air pressure drops.

Finally, we tested the sensitivity of the ice load and the ice deposit diameter to variations of the median volume droplet diameter, from 10 to 50  $\mu\text{m}$ . Figure (2.6) shows the result.

In Figure (2.6) we see that the ice load increases monotonically with an increase in the median volume diameter. However, the ice deposit diameter peaks near a median volume droplet diameter of around 25 $\mu\text{m}$ . This behaviour is related to the duration of the accretion event. When the accretion duration is short, the ice deposit diameter reaches its peak at a small value of the median volume droplet diameter. When the accretion duration

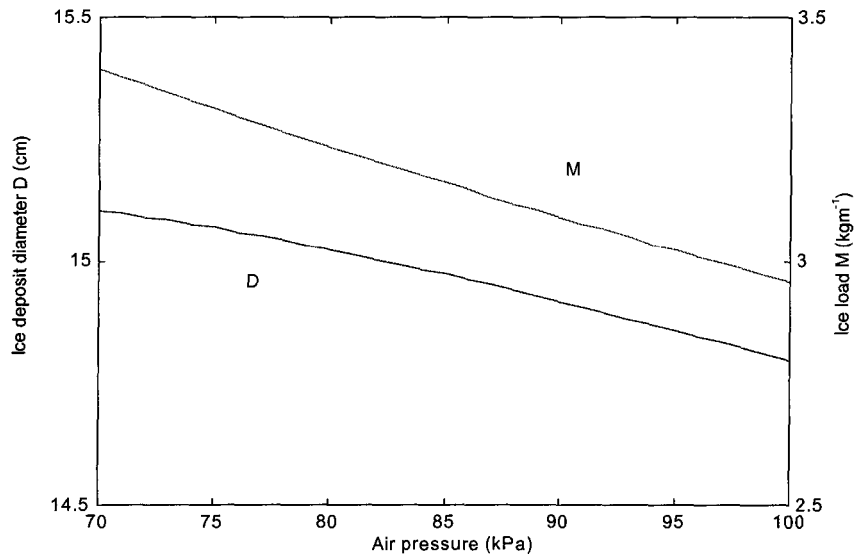


FIG. 2.5. Sensitivity of the ice load  $M$  and the ice deposit diameter  $D$  to variation of the air pressure. Other environmental conditions are as in Fig. 2.4

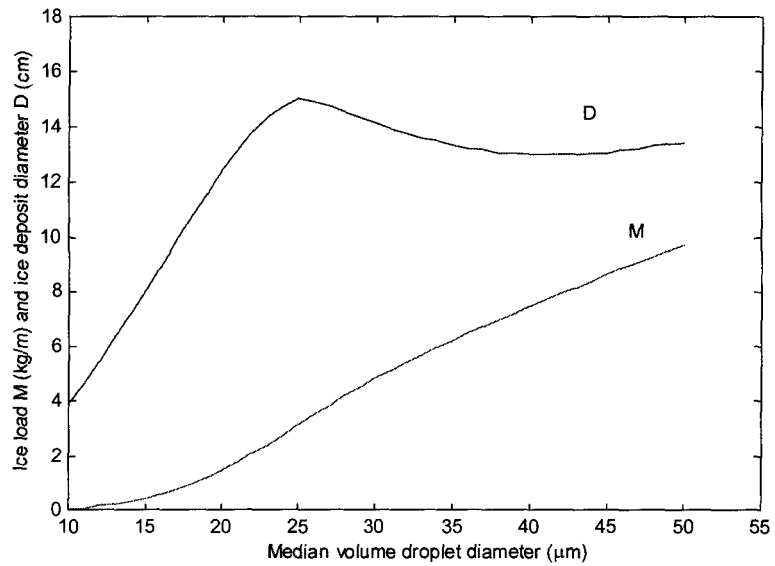


FIG. 2.6. Sensitivity of ice load  $M$  and ice deposit diameter  $D$  to variation of the median volume droplet diameter  $d_m$  ( $\mu\text{m}$ ). The other environmental conditions are as in Fig. 2.4

is sufficiently long (about 168 hours or greater), the peak disappears, and the ice deposit diameter curve becomes increasingly monotonic.

The main contribution of Makkonen's model has been to describe qualitatively the physics of rime ice accretion on wires, and to provide a conceptual framework for the development of quantitative estimation and prediction methods.

### 2.3 The Szilder random walk model

Despite significant progress in their development, classical continuous icing models cannot simulate the complexity of the ice structure and its shape, especially when the ice accretion is large and pendant ice forms under wet conditions. Instead, they typically either assume a simple shape (e.g. Makkonen, 1984), or try to predict ice shapes of limited complexity (e.g. Lozowski et al., 1983). The true complexity of large ice accretions leads to a number of important physical effects which may tend to increase the ice load. The most challenging cases occur when the accretion is very wet and has a complex geometry (including icicles) that changes with time.

Following up an original idea presented by Lozowski et al.(1983), Szilder (1993) introduced the random walk method into ice accretion research, allowing the simulation of wet cases, when unfrozen water may flow a significant distance along the surface of an ice accretion before freezing. The random walk model (also known as a morphogenetic model because it predicts the accretion shape) builds up an ice accretion structure using discrete impinging particles. These particles emulate impinging drops. Each particle can move along the surface of the ice accretion prior to freezing. The parameters controlling the

surface motion and the freezing of the particles are functions of atmospheric conditions. The random walk model also adds some “realistic” stochastic variability to ice accretion shapes.

A two-dimensional analysis of ice accretion on a cylinder using a random walk model was presented by Szilder (1994). A version of the model that allows the prediction of ice accretion on complex, three-dimensional objects has also been developed (Szilder and Lozowski, 1995a). Wind tunnel verification of the model for the formation of a single icicle was described by Szilder et al. (1995c). Finally, a three-dimensional model used to predict the ice accretion on an insulated cylinder under freezing rain conditions has also been formulated by Szilder et al. (1999).

One challenge for random walk models, as with all icing models, is the verification of their simulations. Laboratory and field data are still too sparse to allow complete testing of such models. Such comparisons are even more difficult in the case of models that predict ice accretion shapes (as well as loads), since quantitative and objective means for comparing observed and simulated ice accretion shapes have not yet been developed.

## CHAPTER 3

### MODEL DESCRIPTION

#### 3.1 The two-dimensional morphogenetic model

A random walk method has been used to simulate ice accretion shapes on a horizontal cylinder in freezing rain (Szilder 1994). In the present author's version of the model, a typical conductor with 35mm diameter has been used in the simulation. We will consider first a model for the prediction of ice accretion on a non-energized conductor exposed to vertically falling raindrops. This will be the reference case.

In the model, a horizontal cylinder, of zero heat capacity and thermal conductivity, is exposed to vertically falling freezing raindrops<sup>1</sup>. A ballistic model determines the location of impact of the fluid element, and the behavior of the fluid element flowing along the surface is modelled by a random walk process. These fluid elements may be imagined to consist of a single raindrop, as part of a raindrop or as multiple raindrops (depending on the raindrop size). They maintain their identity as they flow along the surface or drip, while merging with the existing accretion when they freeze.

The simulation domain is defined by a two-dimensional rectangular lattice. The icing substrate is defined by filling appropriate lattice cells. In the reference case, fluid

---

<sup>1</sup> In the present version of the model, the "raindrops" are referred to as "fluid elements". These fluid elements have a volume of  $1 \text{ mm}^3$  (when frozen), and so have a volume about twice that of a raindrop with diameter equal to the typical volume median diameter for freezing rain. In the future, it may be possible to incorporate a realistic droplet size spectrum into the model.

elements are fired from a random position along a horizontal line along the upper edge of the lattice. Prior to impact, their trajectory is taken to be a straight line. An element impinges directly onto the existing ice accretion when it reaches a lattice location just above or to the immediate right or left of a lattice box, which is already occupied by an ice element or an element of the icing substrate. From there, the element begins a random walk.

At each time step during the random walk, there are four possible alternatives for a fluid element: it may move one cell to the right, left or down (diagonal motion is not allowed), or it may freeze. The probabilities for the occurrence of each of these four events are specified. The freezing probability is expressed as a function of atmospheric conditions using a simple analytical approach. In order to simplify the dynamics, the probabilities of motion in the three allowed directions are assumed to be equal. Since the sum of all four probabilities is unity, the probability of motion in any of the three permitted directions is therefore one-third of the difference between unity and the freezing probability. The particle is constrained not to move into an already occupied cell, nor to move to a cell with no occupied neighbours. The latter constraint prevents the particle from walking away from the existing ice or substrate surface.

Having specified the model probabilities, the particle's actual next move is determined using a random number generator with a uniform distribution between 0 and 1, along with a piecewise-linear cumulative probability distribution for the particle's behaviour.

A fluid element's random walk may end in one of two ways. The first is by freezing. This happens if a random number corresponding to the freezing probability interval is

drawn. However, the particle does not necessarily freeze in its present grid cell. Instead a "cradle" location is sought for the element in the neighbourhood of its present location. The size of this search zone is determined by the freezing range parameter,  $n$ . The search neighbourhood is a square centred on the initially determined freezing cell with side length (in cells) equal to  $2n + 1$ . The freezing particle is moved to the empty cell within this area where it will have the maximum number of occupied neighbours (effectively the lowest surface energy). If there is more than one such location, the final site is chosen randomly from among them. We believe that this process emulates the effect of surface tension forces, which tend to minimize the local surface energy. Using numerical experiments, it has been established that for smaller values of the freezing range parameter, the structures has a substantial number of voids. On the other hand, very large values of the freezing range parameter produce ice surfaces with almost no surface roughness, which is unrealistic. In the following calculations, the freezing-range parameter is taken to be 4. According to Szilder (1993), this value gives a good correspondence between the observed and the measured porosity of the ice accretion.

A second possibility for terminating the fluid element's motion is shedding from the ice structure. This may occur in the model only if the element reaches the lowest level of the accretion. If the element remains at the lowest level without freezing for more time steps than a critical value called the shedding parameter, it then drips from the structure. Once a fluid element's motion is terminated, either by freezing or by dripping, the next element is released.

Using a simple analytical approach, the freezing probability and the shedding parameter will be related to the atmospheric conditions and the geometry of the problem.

### **The freezing probability**

The freezing probability may be expressed as follows:

$$P_f = \frac{\Delta l}{0.5L} P_c \quad (3.1)$$

where  $\Delta l$  is the step length measured along the accretion surface (m);  $L$  is the distance along the cylinder surface at which all the water has frozen (m); and  $P_c$  is the probability of motion along the accretion surface. Equation (3.1) may be understood by considering a simple case where the fluid element at each time step moves one cell downward along a vertical wall and consequently  $P_c = 1$ . In this case, the freezing probability is the ratio of the distance covered in one step to the mean length of the element's motion before freezing, i.e. half the distance required for all the water to freeze. When motion around a cylinder is considered, there are two problems that complicate this simple picture. First, fluid elements do not move along the cylinder surface in only one direction at each time step. Secondly, the step length tangent to the cylinder surface does not correspond to the lattice spacing.

In order to estimate the actual probability of motion along the cylinder surface, a series of 1000 numerical experiments was performed. In each experiment, the freezing probability was set to zero and the probabilities of left, right and downward motion were each set to one-third. A fluid element was released from the top of a cylinder oriented vertically whose radius was 17.5 times the grid cell size. In the experiment, because of the

horizontal motion, the average number of steps required to reach the bottom of the cylinder was 373. The number of grid cells over the same vertical distance was 72. Consequently, the probability of motion in the vertical along the cylinder surface, for the assumed values of the directional probabilities, was 0.193.

The relationship between the step length measured along the cylinder surface  $\Delta l$  and the grid size  $\Delta x$  can be written:

$$\Delta l = \Delta x \frac{\pi}{4} \quad (3.2)$$

Equation 3.2 can be understood as follows. Since a fluid element is constrained to travel in either horizontal or vertical steps, it must travel a total distance  $4R$  ( $R$ , the cylinder radius) in order to get half way round the circumference, namely  $\pi R$ . In order to do this in an integral number of steps, Equation (3.2) must be fulfilled.

The distance over which all of the flowing water freezes may be determined using an energy balance equation. The heat loss to the air is proportional to the amount of freezing water:

$$ql = (w\rho_w R - m_l)L_f \quad (3.3)$$

where  $q$  is the mean convective heat flux ( $\text{Wm}^{-2}$ ),  $l$  is the distance measured along the cylinder surface from the upper stagnation line (m),  $w$  is the rainfall rate in  $\text{ms}^{-1}$ ,  $\rho_w$  is the water density in  $\text{kgm}^{-3}$ ,  $m_l$  is the mass flux at location  $l$  ( $\text{kgm}^{-1}\text{s}^{-1}$ ), and  $L_f$  is the latent heat of fusion ( $\text{Jkg}^{-1}$ ). Equation (3.3) takes a simpler form when we consider the location  $l = L$  where on average all the water has frozen. If  $l = L$ , then  $m_l = 0$  and so:

$$L = \frac{w\rho_w RL_f}{q} \quad (3.4)$$

Using Equations (3.2) and (3.4), the freezing probability may be expressed as:

$$P_f = \frac{\pi}{2} \frac{q}{w\rho_w L_f} \frac{\Delta x}{R} P_c \quad (3.5)$$

Thus, the freezing probability is seen to be a function of the following variables: atmospheric conditions, namely convective heat flux and precipitation rate, and the ratio of the grid size to the cylinder radius. This expression for the freezing probability has been derived for a bare cylinder but, for lack of a more complete analysis, it is also used during the growth of the ice accretion.

### The Shedding Parameter

The shedding parameter, which emulates the behaviour of a pendant drop, may also be expressed as a function of the atmospheric conditions. The pendant drop is assumed to behave in a three-dimensional fashion, even though the accretion itself is two-dimensional. Hence, the mass-balance equation for the pendant drop may be written:

$$\int_0^{M_{CR}} dM = \int_0^T 2m_l dt \quad (3.6)$$

The pendant drop starts to form at  $t = 0$  and, after a period  $T$ , its mass reaches a critical value  $M_{CR}$ , at which point it drips off the accretion and the process repeats itself.

The factor of 2 in Equation (3.6) allows for the fact that water flows into the pendant drop from both sides of the accretion. In view of Equation (3.3),  $m_l$  may be written in the form:

$$m_l = w\rho_w R - \frac{ql}{L_f} \quad (3.7)$$

Since the pendant drop forms at a well-defined location ( $l = \text{constant}$ ) for a given time interval, this mass flux is independent of time. This means that the average time interval for a fluid element to stay at the tip of the accretion, as part of the pendant drop, is half the drip period.

The shedding parameter is defined as the average number of time steps,  $\Delta t$ , during which a fluid element stays at the tip of the accretion before dripping. Hence

$$Sh = \frac{0.5T}{\Delta t} \quad (3.8)$$

Calculating the period of dripping from Equation (3.6) and using Equation (3.7), the shedding parameter may be written:

$$Sh = \frac{M_{CR}}{4\Delta t w \rho_w R \left(1 - \frac{l}{L}\right)} \quad (3.9)$$

Thus, the shedding parameter increases with increasing length of the accretion. This result can be explained by the fact that, as the accretion grows, an increasing amount of water freezes on the sides of the accretion, and there is a decrease in the water flux reaching the tip of the accretion. Consequently, more time is required to reach the critical mass. As

the accretion length approaches the maximum length,  $l \rightarrow L$ , the shedding parameter tends to infinity.

The critical mass of the pendant drop can be estimated from experimental data. The measurements show (e.g., Maeno and Takahashi, 1984, Chung and Lozowski, 1990) that the diameter of a pendant drop is approximately 5 mm, and hence its mass is  $6.5 \times 10^{-5}$  kg. The distance between pendant drops formed under a horizontal cylinder is approximately 21mm (Makkonen and Fujii, 1993). Consequently, the critical mass  $M_{CR}$  is estimated to be  $3.2 \times 10^{-3}$  kgm<sup>-1</sup>. The velocity of the fluid elements moving along the accretion surface is taken to be 10 mms<sup>-1</sup>. Hence the time step  $\Delta t$  corresponds to 0.1 s.

### 3.2 Model modification for considering the Joule heating effect

When electrical current flows in the conductor, the Joule heating effect can be an important factor affecting the ice accretion. The electrical resistance of bare stranded conductor varies with frequency, average current density and temperature. For our purposes, we assume that the current transferred within the conductor is constant. Changes of the electrical resistance due to temperature changes are ignored.

In this thesis, we adopt a naive approach to Joule heating, by simply adding it to the external, environmental heat transfer, the difference being the net heat transfer that determines the ice accretion rate. This assumption ignores the important distinction that Joule heat is applied on the inner surface of the ice while environmental heat transfer applies at the outer surface. Consequently, the results presented here are intended to be illustrative, losing their validity as the ice accretion becomes very large.

When allowing for Joule heating, we therefore consider that the sum of the heat loss to the air and the heat generated by the electric current is proportional to the rate of freezing. Consequently Equation (3.3) is modified as follows:

$$(q - I^2 R_E / 2\pi R)l = (w\rho_w R - m_l)L_f \quad (3.10)$$

where  $I$  is the electric current (A) and  $R_E$  is the resistance of the conductor ( $\Omega\text{m}^{-1}$ ). The other symbols are same as in Equation (3.3). This equation is suitable to describe the heat balance at the surface of the conductor during the initial steps of the formation of the ice accretion. Nevertheless, for illustrative purposes only, it has been used for the entire ice accretion event.

Equation (3.10) takes on a simpler form when the location  $L$  where all the water has frozen is considered. If  $l = L$ , then  $m_l = 0$  and so:

$$L = \frac{w\rho_w RL_f}{(q - I^2 R_E / 2\pi R)} \quad (3.11)$$

Using Equations (3.9) and (3.11), the freezing probability may be expressed as:

$$P_f = \frac{\pi (q - I^2 R_E / 2\pi R)}{2 w\rho_w RL_f} \Delta x P_c \quad (3.12)$$

Once the heat balance equation has been adjusted, in view of the Equation (3.11), the Joule heating effect also affects the shedding parameter by changing the value of  $L$  in Equation (3.9).

### 3.3 Model modifications for considering variable drop impingement angles

Previous random walk models have simulated the ice accretion on a cylinder exposed to vertically falling rain. Under real atmospheric conditions, the occurrence of glaze is always accompanied by wind. Apart from its effect on the surface convective heat transfer conditions, the wind can also influence the raindrop impact angle and the motion of the fluid elements during their random walk. The simulation of ice accretion under wind-influenced drop impingement angles is included in the current model.

In order to accomplish this, we modified the ballistic model which determines the impact location of the fluid elements. Fluid elements are now fired from a random position along a straight line that is inclined to the horizontal line on the upper boundary of the lattice. The distance between the centre of the line and the centre of the icing substrate is always kept the same no matter how the inclined angle changes. Subsequently, the fluid elements follow oblique straight trajectories which make the same angle with the vertical. This angle is defined to be the droplet impingement angle  $\phi$ . The exact lattice trajectory taken by each ballistic fluid element is calculated using appropriate simple geometrical equations. An element impinges onto the existing ice accretion when it reaches a lattice location just above or to the immediate right or left of a lattice box which is already occupied by an ice element. From this point, the element begins its random walk.<sup>2</sup>

---

<sup>2</sup> It should be noted here that, for simplicity we do not try to emulate all of the details of droplet impingement. For example in nature, drops of different size will impinge at different angles. This could be an important effect to account for because it means that drops of different sizes will effectively “see” different accretion cross-sections. Instead, we assume, for simplicity that all drops are of equal size and fall at the same angle. We take that size to be the median volume diameter, although it could be argued that it should be the median flux diameter. We also ignore any splashing of liquid upon impingement.

At each step during the random walk of a fluid element, the freezing probability is kept constant. We try to emulate the effect of wind stress on the fluid motion as follows. The ratio of the difference between the probabilities of leftward and rightward motion (which are now no longer equal) to the probability of downward motion is set equal to the tangent of the droplet impingement angle  $\phi$ . The sum of all three probabilities plus the freezing probability is unity. This formulation will need to be validated and re-visited in the future. It is especially difficult to apply in two-dimensional simulations, because the effect of wind stress in two-dimensions may be to modify the vertical motion as well as the horizontal motion of surface liquid.

We take a simple approach to find the impingement angle  $\phi$  of a “representative” drop (the median volume diameter drop). The full droplet spectrum and turbulent fluctuations in wind speed and direction are not considered here. Rather the wind is considered to be steady, horizontal and perpendicular to the conductor, and a mono-disperse droplet spectrum is assumed.

For raindrops, an empirical equation proposed by Atlas et al., based on the data of Gunn and Kinzer (1945), can be used to estimate the raindrop terminal velocity,  $V_T$ (m/s):

$$V_T = 9.65 - 10.3e^{-0.6D} \quad (3.13)$$

When the wind speed is  $V_W$  ( $\text{ms}^{-1}$ ), and the terminal velocity  $V_T$  is given by equation (3.13), the total impingement velocity,  $V_D$ , and the impingement angle,  $\phi$ , can be obtained by a vector sum (Figure (3.1)).

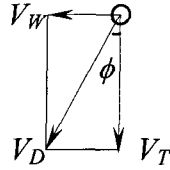


FIG. 3.1 Diagram of the raindrop velocity showing the impingement angle  $\phi$ .

$$\phi = \tan^{-1}\left(\frac{V_W}{V_T}\right) \quad (3.14)$$

The median volume drop diameter is used here to typify the rain drop size distribution. However, as mentioned above, the median flux diameter may in fact be more appropriate. Nether choice, however, will adequately simulate the outcome of using the full spectrum of droplet sizes, fall speeds and impact angles.

Mason (1971) proposes the following relation between median volume diameter,  $D(\text{mm})$ , and precipitation rate,  $W (\text{mmh}^{-1})$  :

$$D = W^{0.23} \quad (3.15)$$

He states that this is “fairly representative of average drop size spectra” for “fairly steady continuous rain produced by the Wegener-Bergeron process”. Freezing rain typically fits this description.

## CHAPTER 4

### MODEL SIMULATION RESULTS AND DISCUSSION

Using fluid elements that are square with a side of 1mm, random walk simulations were performed on a two-dimensional lattice consisting of 100 by 150 grid cells, each with a side of 1mm. Model calculations show that a change in the temperature of the drops within a realistic range does not substantially influence the accretion shape. In the results presented here, the drop temperature is assumed to be +2 °C (Szilder, 1994). Since the ice growth is wet, it is assumed that the ice density is  $900 \text{ kgm}^{-3}$ . The model was used first to simulate the ice accretion on a non-energized transmission line conductor, exposed to vertically falling raindrops.

#### 4.1 Model predictions of freezing rain accretion on a non-energized conductor

##### 4.1.1 Model predictions analyzed as a function of convective heat flux

Using the model, the influence of external heat flux has been investigated first. In general, the external heat flux consists of convective, evaporative and radiative terms. However, for convenience, we will simply refer to the sum of these as the convective heat flux. A precipitation rate of  $5\text{mmh}^{-1}$  and a 5 hour icing event duration were used in the simulation.

Examples of the accretion shapes for increasing values of the convective heat flux are shown in Figure (4.1). In this figure, consecutive ice layers formed during three

successive 100 minutes time steps are distinguished using different symbols. It should be noted that for now we have assumed a torsionally stiff cylinder, which is not subject to rotation. An example of an accretion shape, in which the ice covers only part of the cylinder's surface after five hours, is shown in Figure (4.1a). The accretion grows gradually with increasing external convective heat flux and the ice layer eventually covers the entire cylinder surface. When the convective-heat flux is  $30\text{Wm}^{-2}$  (Figure (4.1b)), an optimum combination of the heat flux and water availability below the cylinder leads to a substantial pendant accretion (icicle). For a convective heat flux of about  $60\text{Wm}^{-2}$  (Figure (4.1c)), almost 80% of the liquid impinging onto the accretion is incorporated into the ice structure and, at this point, the accretion length reaches a maximum. At still higher values of the convective heat flux, the accretion mass on the upper half of the cylinder increases, and hence the overall length of the accretion decreases, and the centre of mass moves upward. The beginning of this process may be seen in Figure (4.1d). Still further increases of the convective heat flux lead to an accretion which is larger above than below the cylinder Figure (4.1e,f). A substantial increase of the cross-section of the accretion leads to an increase in the rate of drop impingement onto the accretion during ice growth. For the sake of academic interest, two accretion shapes under unrealistic convective heat fluxes, 500 and  $1000\text{Wm}^{-2}$ , are shown in Figure (4.1g, h). At such high heat fluxes, most of the impinging liquid freezes on the upper half of the cylindrical cable.

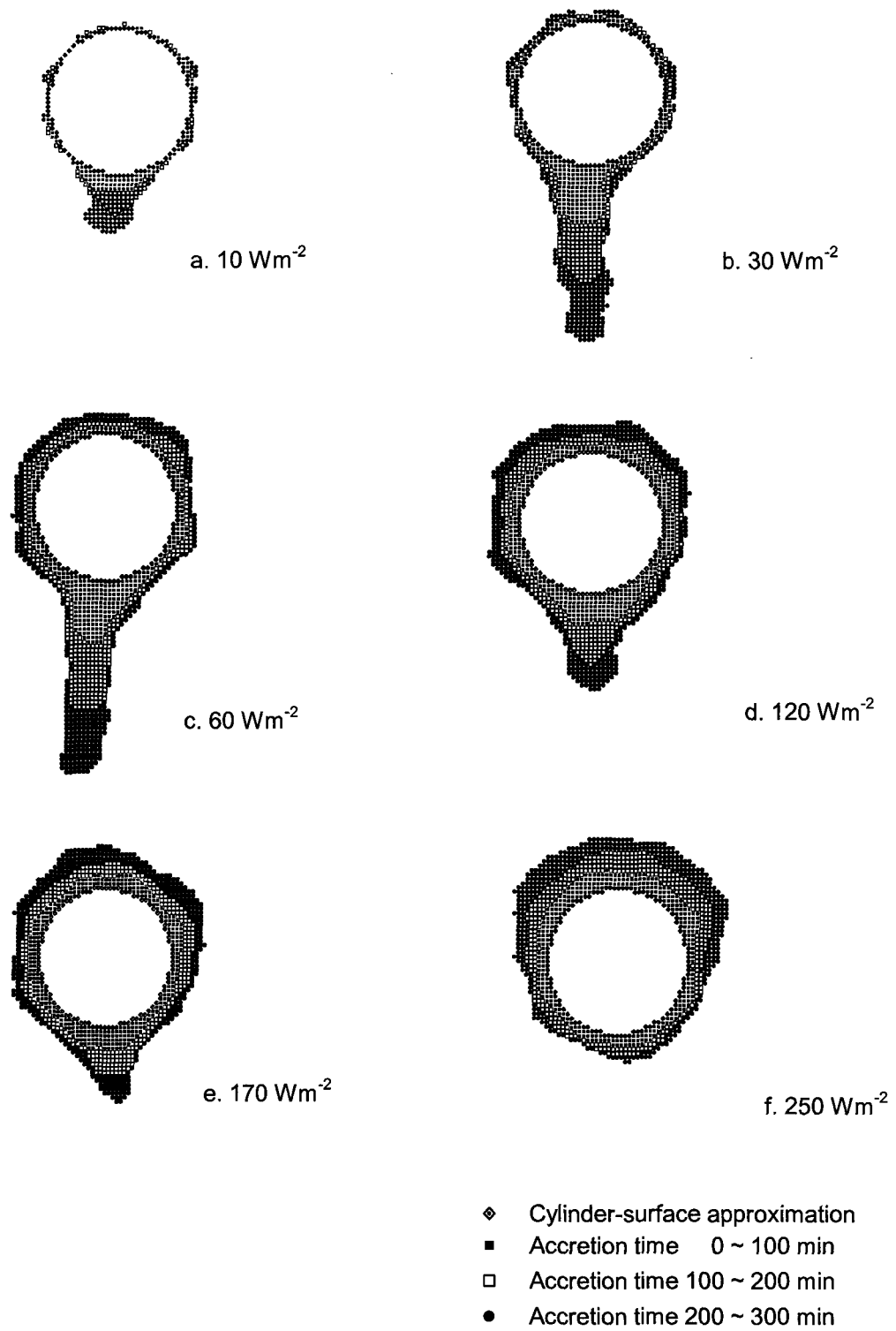


FIG. 4.1 The influence of the convective heat flux on the shape of the ice accretion. The following parameter values have been assumed: rainfall rate  $5\text{mmh}^{-1}$ , drop temperature  $+2^\circ\text{C}$ , simulation time 5h.

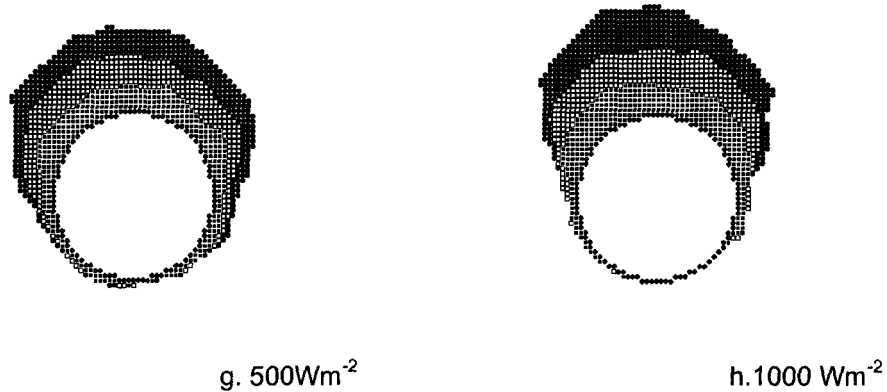
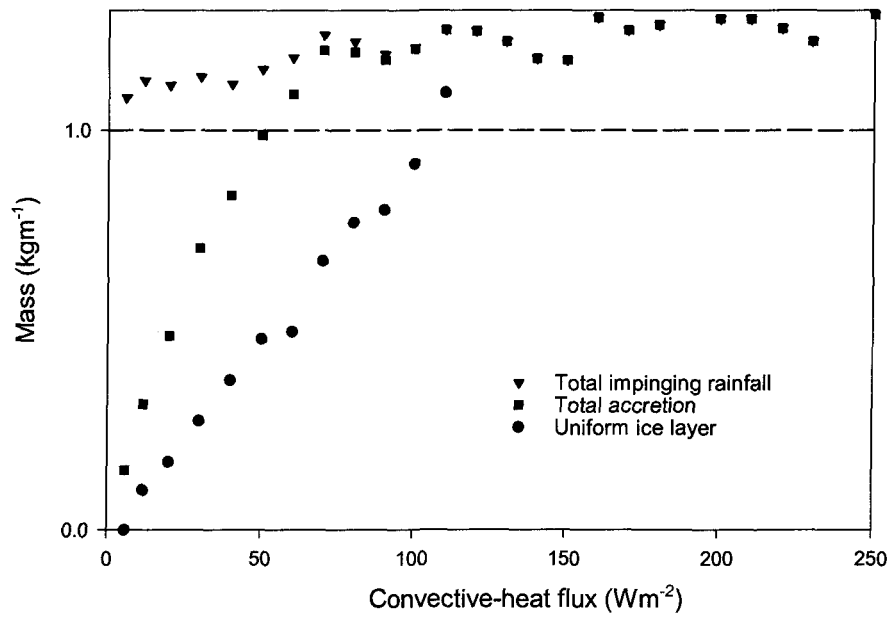
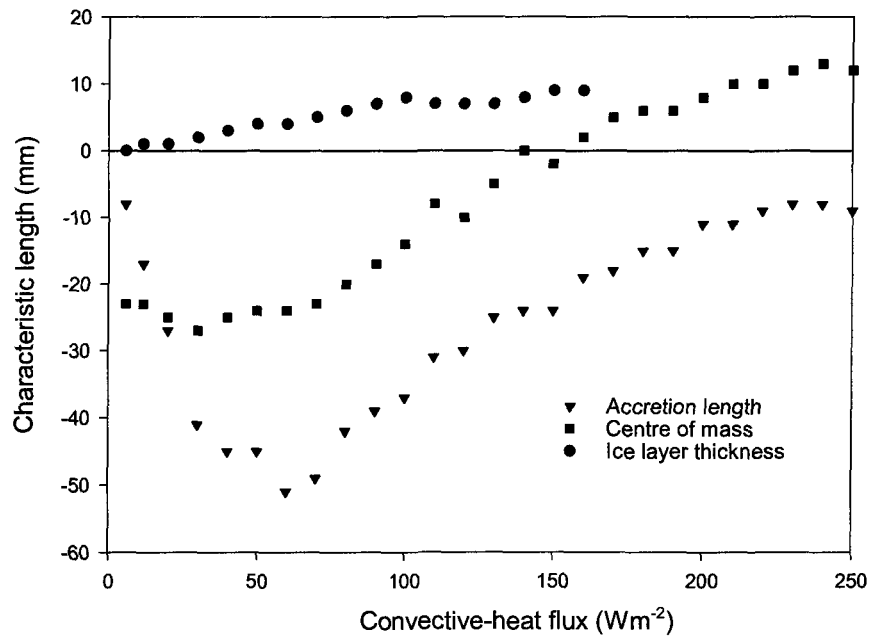


FIG. 4.1 Continued

The influence of the convective heat flux on the distribution of the mass of the ice accretion is shown in Figure (4.2a). The total impinging rainfall mass increases slowly with increasing heat flux, since the cross-section of the accretion, which intercepts the rain, also increases with external heat flux. Initially, the total accretion mass increases rapidly with rising heat flux, until it eventually equals the total impinging rainfall mass, at which point all of the impinging water freezes somewhere on the accretion. The “uniform ice-layer mass”, calculated as twice the mass accreted on the upper half of the cylinder, increases almost linearly with heat flux. Once the accretion mass on the upper half of the cylinder exceeds the accretion mass below the cylinder, the uniform ice-layer mass is not displayed.



(a)



(b)

FIG. 4.2. The influence of the convective heat flux on the accretion process: (a) Variation of the three characteristic masses (b) Variation of the three characteristic lengths.

The length growth behavior is more complex. On the one hand, an increase of the heat flux will lead to the potential for faster freezing at the icicle tip, since less liquid is lost by shedding. On the other hand, there will be less water available to freeze at the tip as a result of enhanced freezing on the upper part of the cylinder and on the icicle walls. Because of these two competing processes, small values of the convective heat flux are associated initially with a small accretion length, and an increase of the heat flux leads to an increase of the accretion length. For still larger values of the convective heat flux, the accretion length actually decreases with increasing heat flux, as more ice freezes on the walls of the icicle and less liquid is available to freeze at the tip.

The vertical coordinate of the accretion's centre of mass, measured upward from the centre of the cylinder, and the pendant accretion length, defined as the distance between the bottom of the cylinder and the lowest part of the accretion, are shown as linear measures of the ice-shape geometry in Figure (4.2b). For very small values of the convective-heat flux, ice forms only on the lower part of the cylinder. With an increase of the convective heat flux, the centre of mass moves slightly downward. A further increase of the convective heat flux leads to upward motion of the centre of mass, which moves to locations above the axis of the cylinder at a heat flux of approximately  $150 \text{ Wm}^{-2}$ .

#### 4.1.2 Model predictions analyzed as a function of precipitation rate

The influence of the precipitation rate on the accretion is also examined in Figure (4.3). The external convective heat flux is assumed to be  $30 \text{ Wm}^{-2}$ . At rainfall rates less

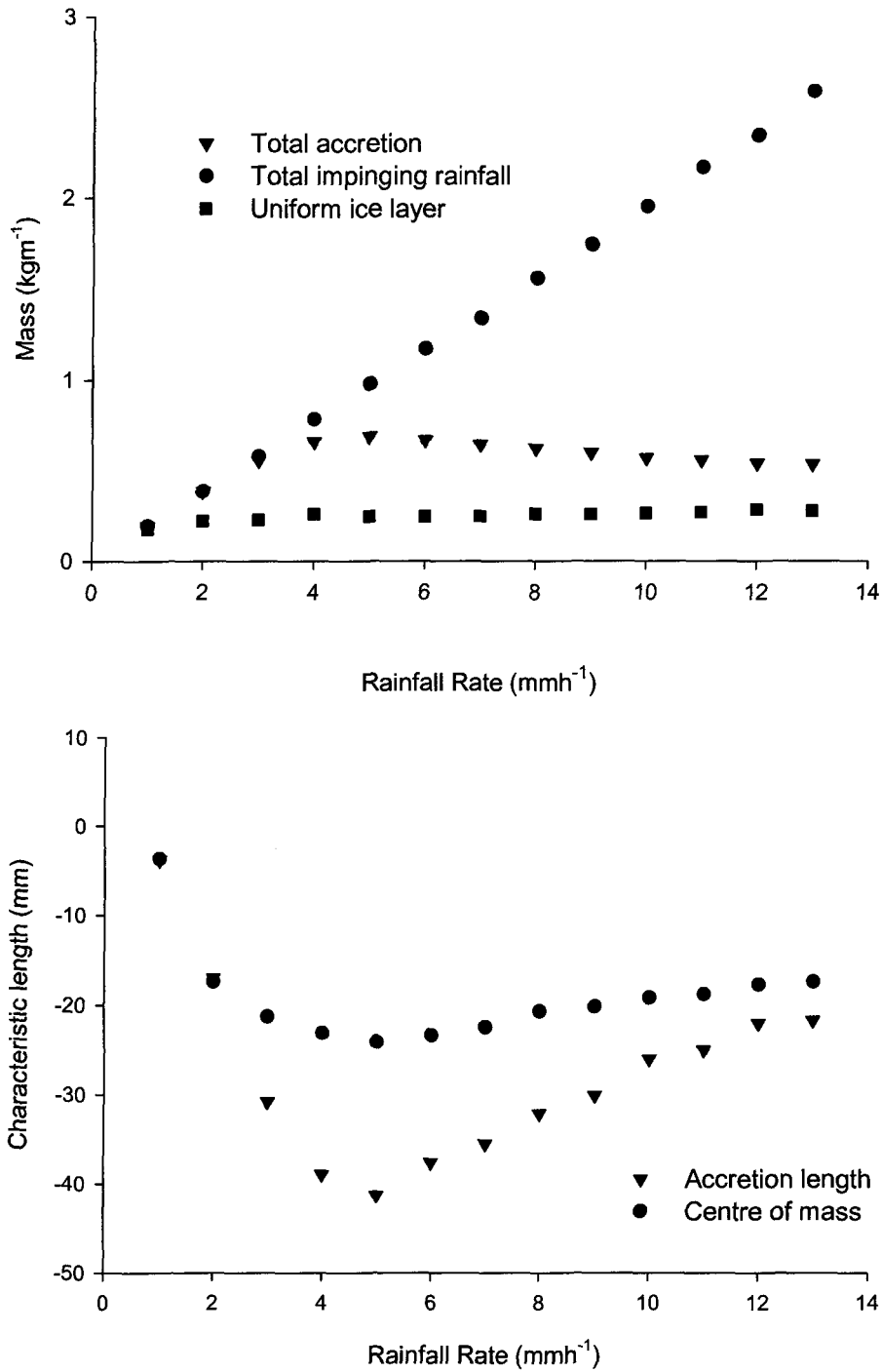


FIG. 4.3 The influence of freezing rainfall rate on the ice accretion characteristics: (a) Variation of characteristic masses (b) Variation of characteristic accretion lengths. The convective heat flux is  $30 \text{ Wm}^{-2}$ .

than  $1\text{mmh}^{-1}$ , the sensible heat brought by the warm rain is small by comparison and the convective heat flux is large enough to quickly freeze all the impinging liquid. Consequently, most of the accretion occurs on the upper half of the cylinder and there is no dripping.

When the rainfall rate is  $1\text{mmh}^{-1}$ , there is sufficient liquid flux to cover the entire cylinder at the end of five hours. A further increase of the rainfall rate does not substantially change the amount of accretion on the upper half of the cylinder, because this is controlled by the external convective heat transfer which is independent of the rainfall rate. Consequently, the mass and thickness of the uniform ice layer remains approximately constant. However, as the rainfall rate increases, the accretion mass below the cylinder also increases. The centre of mass moves downward and some of the drops begin to fall from the tip of the icicle. At a rainfall rate of  $5\text{mmh}^{-1}$ , the accretion length (icicle length) reaches a maximum. The existence of two competing processes can explain the occurrence of this maximum. A low impinging water flux means that there is the potential for more water to freeze. On the other hand, a large impinging flux means that more sensible heat is brought by the warm drops and the pendant drops drip faster. The result is that much of the additional rainfall is lost through dripping. A further increase in the rainfall rate leads to a gradual decrease in the accretion length below the cylinder. Consequently, the centre of mass of the accretion moves upward. The process of a diminishing accretion below the cylinder with a more-or-less constant accretion on top of the cylinder continues as the rainfall rate continues to increase. Finally, a further increase in the rainfall rate leads to the disappearance of ice from the top of the cylinder, because of the high sensible heat flux.

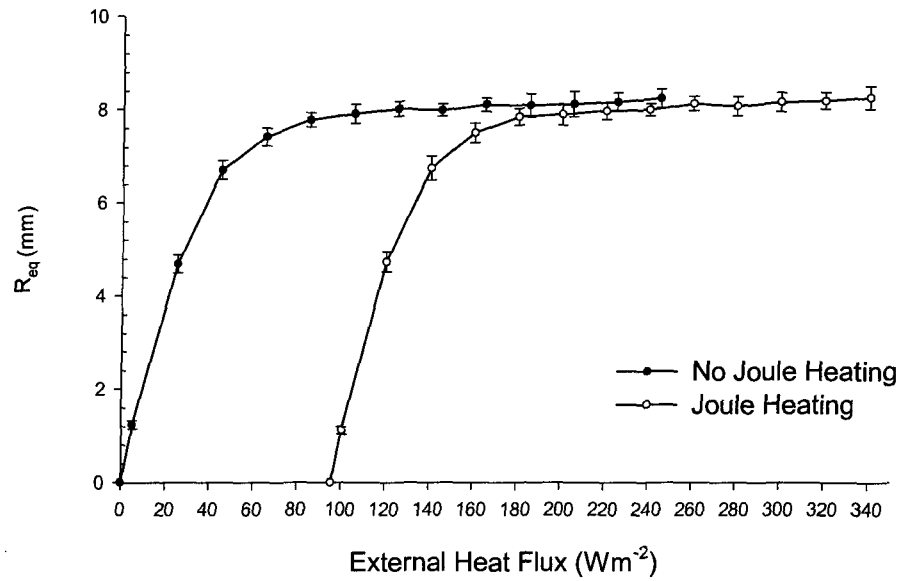
Since such a rainfall rate seems to be unrealistically high for freezing rain, these results are not shown here.

#### 4.2 Model predictions with consideration of the Joule heating effect

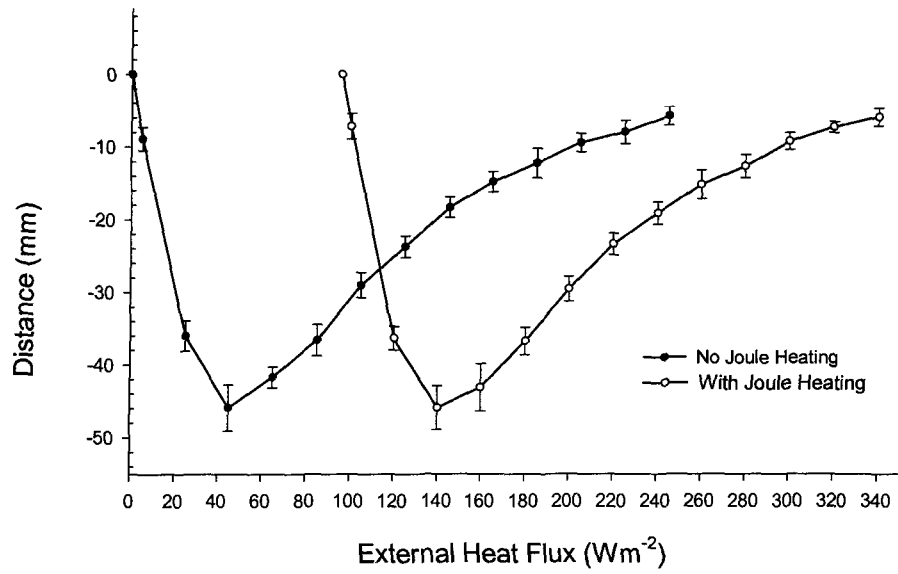
The Hydro Québec ACSR (aluminum conductor steel reinforced) transmission line conductor “Bersimis” has been used as the reference for the present simulation. For the “Bersimis” transmission line conductor, when operated at 315kV, a typical electric current is 500~700A. 500A is assumed in the simulation. In order to simplify the calculation of energy dissipation, a constant value of electrical resistance is assumed and taken to be  $4.21 \times 10^{-5} \Omega \text{m}^{-1}$ . Consequently, the heat dissipation by Joule heating is  $95.4 \text{ Wm}^{-2}$ . Again, a  $5 \text{ mmh}^{-1}$  precipitation rate and a 5-hour simulation time were used in the simulation.

As before, the influence of external heat transfer is investigated first. Due to the Joule heating effect, no ice accretion will occur on the conductor surface unless the external heat flux exceeds the Joule heat flux. Once the external convective flux offsets the heat generated by the electric current, ice accretion will appear on the upper side of the conductor. A further increase of the external convective flux leads to the appearance of an icicle accretion.

In Figure (4.4a), the equivalent radial ice thickness is shown as a function of the external convective heat flux both with and without Joule heating. Equivalent radial ice thickness is defined as the thickness of the total accretion mass if it were distributed uniformly around the conductor. For each case we ran the model 10 times, using different initial seed values for the random number generator. The model parameters remained fixed



(a)



(b)

FIG. 4.4 The influence of the external convective heat flux on the ice accretion under the simulations without and with Joule heating effect. Rainfall rate  $5mmh^{-1}$ , simulation time 5 h. The error bars are the standard deviations of the results for 10 runs of the model (refer to the text). (a) Equivalent ice thickness as the function of external convective heat flux. (b) The accretion length as the function of external convective heat flux.

for each of these runs. The means (points) and the standard deviations (error bars) of the results are shown in Figure (4.4). The ice accretion on the conductor, with Joule heating, appears once the external convective heat flux reaches  $95.4 \text{ Wm}^{-2}$ . Initially, the equivalent radial ice thickness increases rapidly as the external heat flux rises. However, once the external convective heat flux is sufficient to freeze all the impinging rainfall,  $R_{eq}$  remains essentially constant despite the increasing external heat transfer. Still further increases of the convective heat flux lead to more accretion forming on the upper half of the cylinder. A substantial increase of the horizontal cross-section of the accretion leads to an increase in the number of drops impinging onto the accretion during accretion growth. The equivalent radial ice thickness increases only very slowly with increasing external convective heat flux in this regime. The accretion lengths for the two cases (with and without Joule heating) are shown in Fig. (4.4b) as a function of the external convective flux. In these figures we see the simulation results as a function of the external convective heat flux. It appears that Joule heating merely shifts the graphs to the right. This can be explained as follows. The heat generated by the electrical resistance of the conductor changes the energy balance of the accretion and leads to the modification of two important parameters in the model – the freezing probability and the shedding parameter. Consequently, when Joule heating is considered in this simple fashion, it leads to the same result as for an unenergized conductor, with a corresponding reduced convective heat transfer. In future versions of the model, it may be possible to consider the Joule heating to take place on the inner surface of the ice accretion, while the convective heat transfer takes place on the outer surface.

### 4.3 Model predictions when considering variable drop impingement angles

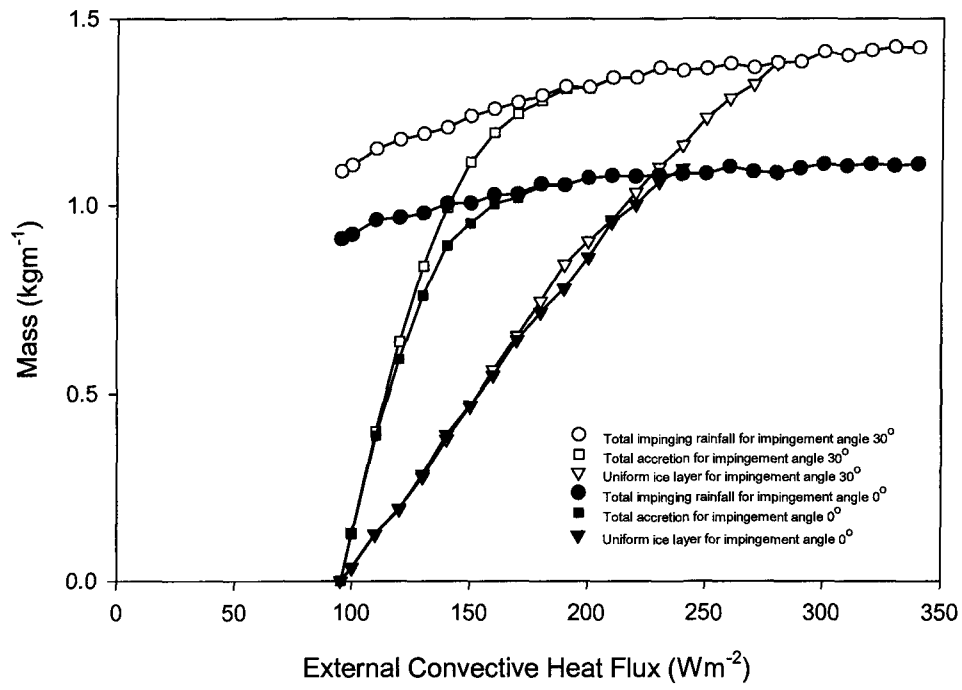
Simulations of ice accretion have been made for an energized transmission line conductor under a range of droplet impingement angles. In each simulation, however, the droplet impingement angle is fixed, implying a constant wind speed and a single droplet size with a fixed fall speed. The influence of the external convective heat flux has been investigated. The transmission line conductor “Bersimis” with the same parameters as in the previous section has been used in the simulation.

#### 4.3.1 The influence of varying impinging raindrop angle on the ice accretion

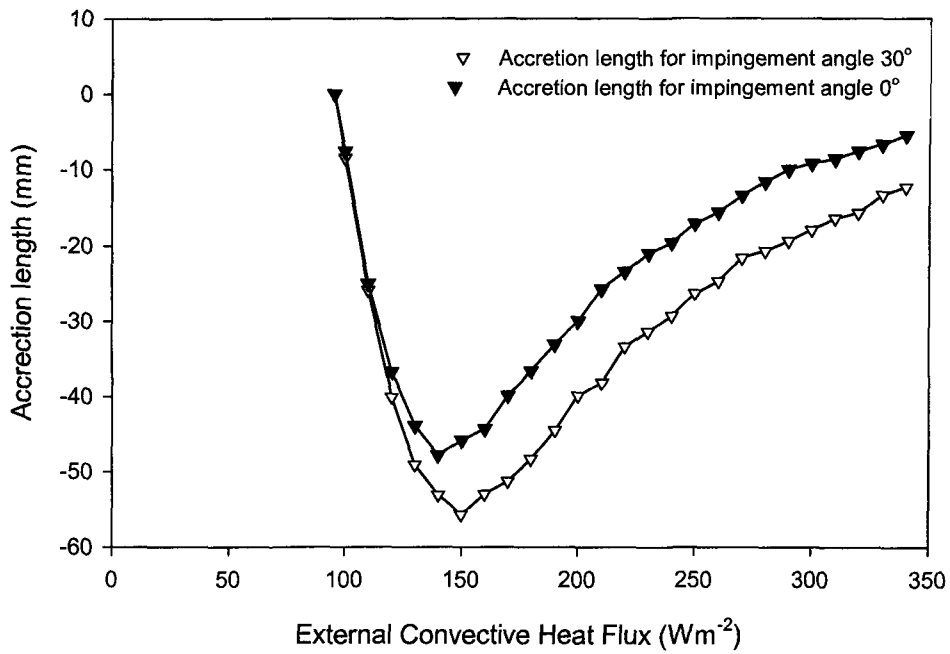
Using Equations (3.13) and (3.14), the impact angle of the single drop size can be determined for a specified wind speed and rainfall rate. In the simulation, we assume that the wind blows horizontally from the right, perpendicular to the conductor, at a speed of  $3\text{ms}^{-1}$  ( $10.8\text{ kmh}^{-1}$ ). Since the rainfall rate is assumed to be  $5\text{mmh}^{-1}$ , the impingement angle is 30 degrees to the vertical. The simulation time is 5 hours.

A comparison of the influence of the external convective heat flux on the mass of the ice accretion for a  $0^\circ$  impingement angle and a  $30^\circ$  impingement angle is shown in Figure (4.5).

From this figure we can see that, for the same rainfall rate, there are more impinging raindrops at a  $30^\circ$  impingement angle than at  $0^\circ$ . The increase is about 25%. This occurs because of the windblown flux. The total accretion mass for both cases increases rapidly with external heat flux initially, and then levels off. The total accretion mass for the  $30^\circ$



(a)



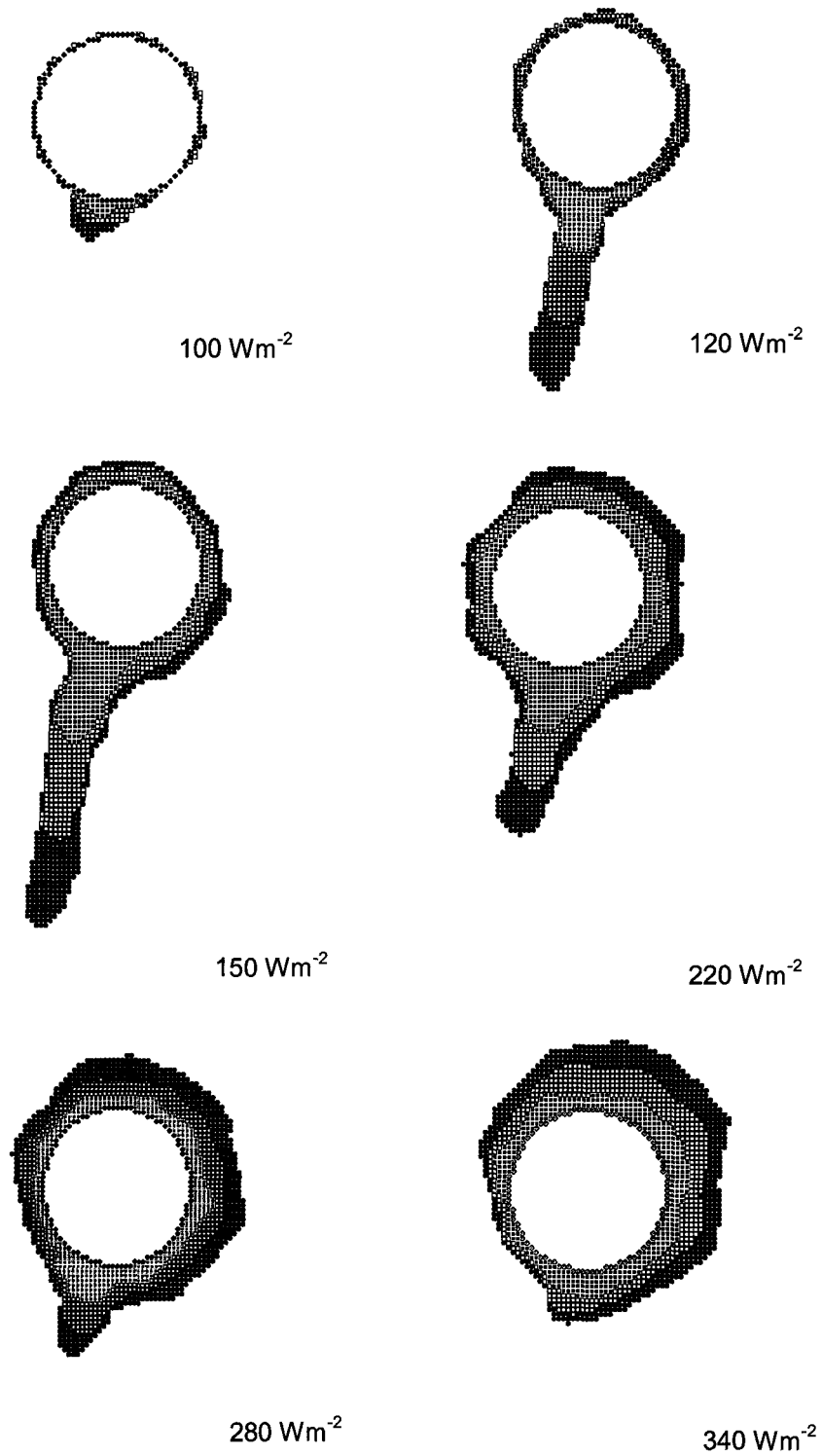
(b)

FIG. 4.5 The influence of the external convective heat flux on (a) the mass of the ice accretion and (b) the accretion length for raindrop impingement angles of 0° and 30°.

case increases faster and reaches a higher asymptotic value than for the  $0^\circ$  case. Once the asymptotic value has been reached, the total accretion mass increases more slowly, but faster for the  $30^\circ$  case than for the  $0^\circ$  case. The uniform ice layer grows at almost the same rate in both cases, suggesting that the main difference between the two cases is due to icicle formation.

These differences may be explained as follows. There are more impinging raindrops and so there is more ice accretion for the  $30^\circ$  case. When the raindrops impinge at an angle, they hit not only the horizontal cross-section, but also the lateral cross-section of the accretion, which is large due to icicle formation. Consequently the total accretion mass increases faster at  $30^\circ$  than at  $0^\circ$ . The accretion lengths for the two cases are shown in Figure (4.5b). The icicle for the  $30^\circ$  case reaches its maximum length at a higher external convective heat flux, and this maximum length is greater than for the  $0^\circ$  case. This difference in length is maintained as the external convective heat flux increases. This result can be explained as follows. Initially, for low external heat transfers, the uniform ice layer mass for the two cases increases at the same rate. Since, as described above, the  $30^\circ$  case accretes more mass because of the higher effective cross-section, more freezing takes place on the pendant part of the accretion (the icicle) and this leads to the accretion becoming longer.

Examples of the accretion shapes for increasing values of the convective heat flux are shown in Figure (4.6). Qualitatively, the development of the ice accretion in the  $30^\circ$  cases is similar to the  $0^\circ$  cases. In these figures, a leftward inclination of the icicles is apparent, especially near the beginning of icicle formation. The angle seems to diminish

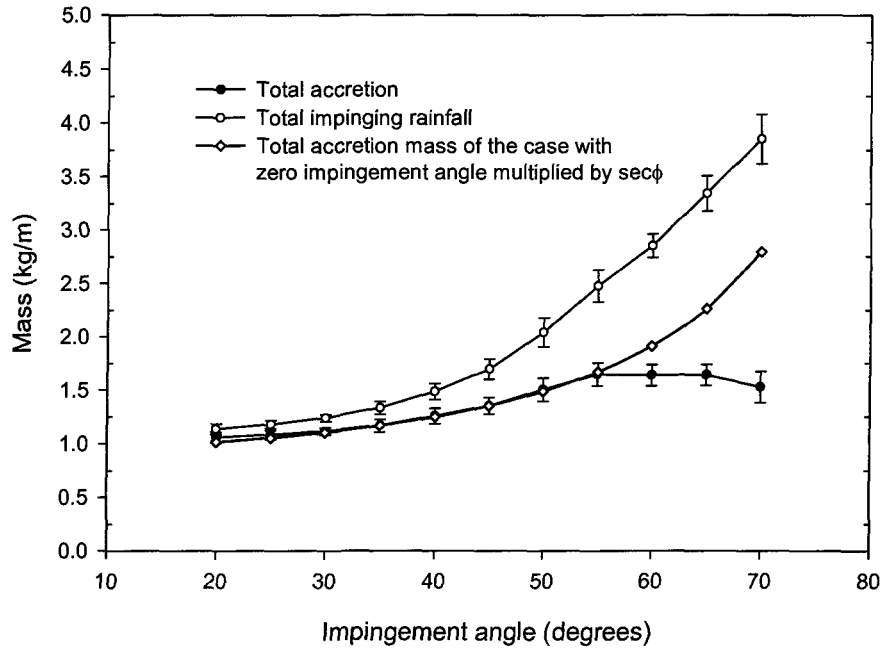


- ◆ Cylinder-surface approximation    □ Accretion time 100 ~ 200 min
- Accretion time 0 ~ 100 min        ● Accretion time 200 ~ 300 min

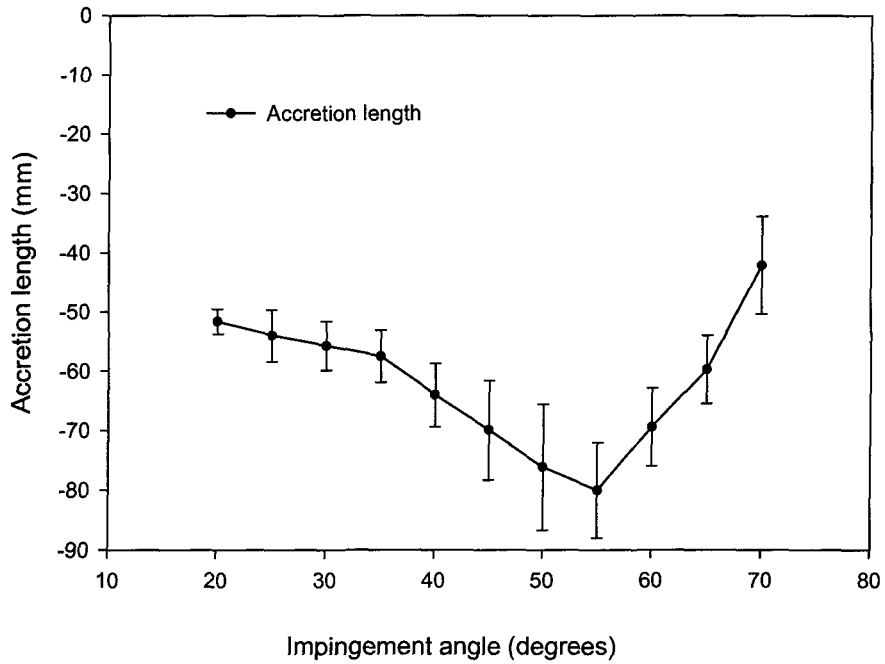
FIG. 4.6. Ice accretion shape development with increasing external heat flux under a  $30^\circ$  raindrop impingement angle. Conductor diameter 35.1mm, rainfall rate  $5\text{mmh}^{-1}$ , simulation time 5h.

with time however. This occurs because, with an increase in icicle length, most fluid elements hit the right lateral surface of the icicle, and from there begin their random walk. Since they are limited to move only in three perpendicular directions, they cannot walk around to the other side of the icicle. Hence the leftward inclination angle of the icicle diminishes with time in some cases. This is probably an artefact of two dimensions, and it would not likely occur to the same extent in three dimensions. In Figure (4.6), consecutive ice layers formed during 100 minutes time steps are represented by changes in shading. These help to visualize the temporal development of the ice accretion under each external heat transfer condition. For a small external convective heat flux, most of the ice accretion lies below the cylinder. Almost all of the new accretion is at the tip of the developing icicle. As the ice accretion begins to form on the upper half of the cylinder, with an increase of the external heat flux, the non-uniformity of the ice accretion development becomes apparent. As shown in the  $340 \text{ Wm}^{-2}$  case, almost all of the new accretion forms on the upstream side of the existing accretion.

The influence of the droplet impingement angle on accretion growth has also been investigated. According to Bell Canada's survey (Collins, 1971. quoted by Stallabrass, 1983), recorded at Toronto International airport over a 10 year period, the maximum and minimum values of mean wind speed during freezing precipitation were  $14.9\text{ms}^{-1}$  and  $1.8\text{ms}^{-1}$  respectively. If the precipitation rate is assumed to be  $5\text{mmh}^{-1}$ , the monodisperse raindrop impingement angle varies from approximately  $20^\circ$  to  $70^\circ$ . For this range, the simulation results for accretion mass and length are shown in Figure (4.7). An external



(a)



(b)

FIG. 4.7. The influence of the rain drop impingement angle on the ice accretion characteristics. (a) Characteristic masses. (b) Accretion length. The error bars are the standard deviations of the simulation results for ten runs with different random number generator seeds.

convective heat flux of  $150\text{Wm}^{-2}$  has been assumed in these simulations, simulation time 5 hours. For simplicity, it was decided to keep the external heat flux constant while changing the impact angle in order to identify their individual effects. However, we recognize that the two will be coupled in nature because both the heat transfer coefficient and the impact angle will depend on wind speed. For a fixed precipitation rate, the total impinging rainfall increases with increasing impingement angle. For comparison purpose, the total accretion mass of the case with zero impingement angle multiplied by  $\sec\phi$  ( $\phi$ , the impingement angle) is also shown. The total accretion mass increases with increasing impingement angle until it reaches its maximum at around  $55^\circ$ . Thereafter, it decreases as the total impinging rainfall increases. The accretion length also reaches its maximum at an impingement angle of about  $55^\circ$ , and then subsequently decreases. For an impingement angle of  $20^\circ$ , 90 percent of the total impinging water freezes. As the impingement angle increases, more impinging water becomes available to freeze, but the greater sensible heat brought by the drops causes the pendant drops to drip faster. The result is that the ratio of total ice accretion mass to total impinging water mass is reduced. For large impingement angles, freezing tends to occur only on the upstream side.

Examples of the accretion shapes for various impingement angles are shown in Figure (4.8). It is apparent that the new accretion tends to form preferentially on the right side of the existing ice accretion as impingement angle increases. As before, the leftward inclination of the icicles in the initial stage of the simulation is greater than during the later stages. The icicle accretion angle does not, however, change dramatically with

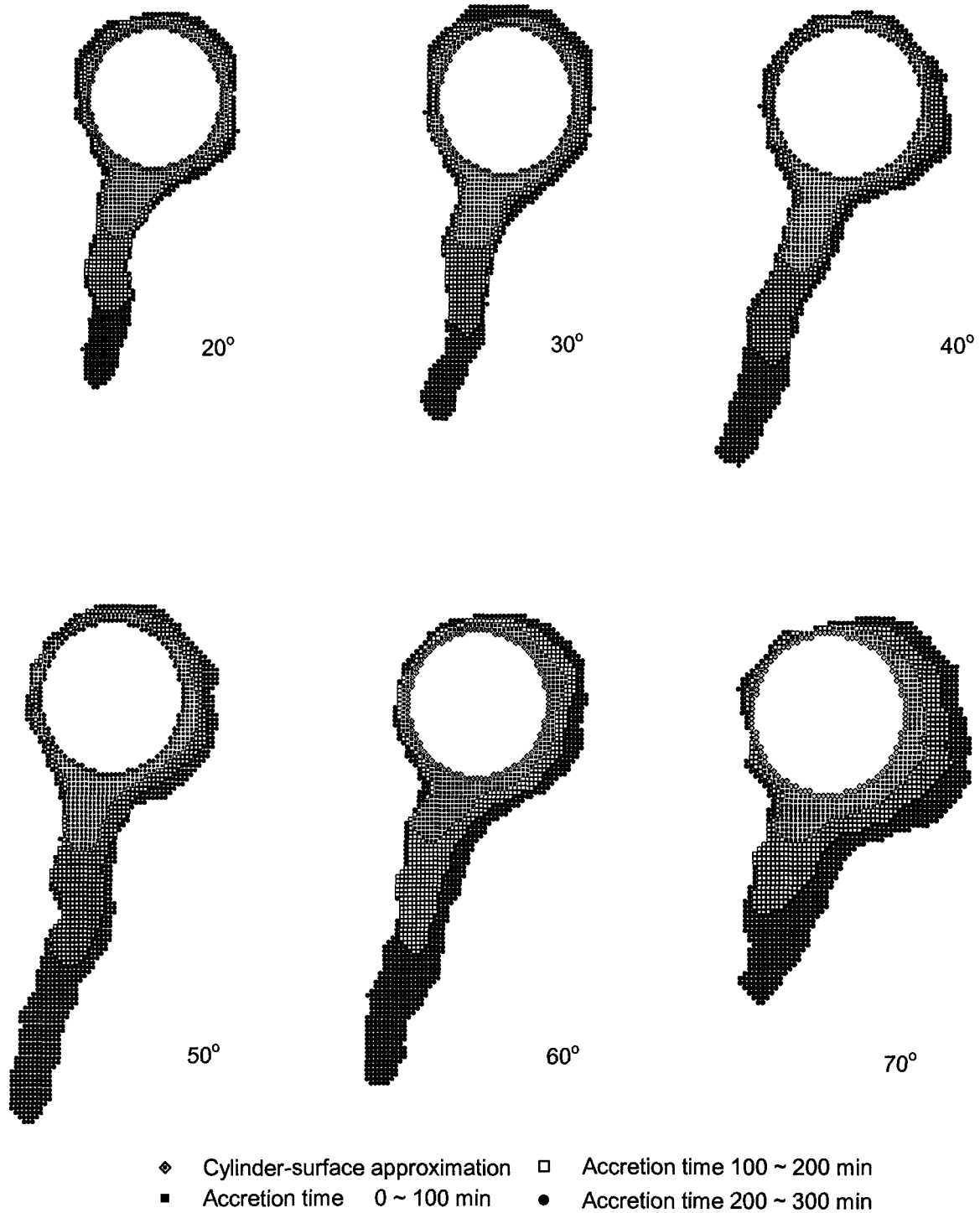


FIG. 4.8. Accretion shapes for simulations with various raindrop impingement angles. External convective heat flux  $150 \text{ Wm}^{-2}$ , precipitation rate  $5 \text{ mmh}^{-1}$ , simulation time 5h. The corresponding to wind speeds are  $1.9 \text{ ms}^{-1}$ ,  $3.1 \text{ ms}^{-1}$ ,  $4.5 \text{ ms}^{-1}$ ,  $6.3 \text{ ms}^{-1}$ ,  $9.2 \text{ ms}^{-1}$ ,  $14.6 \text{ ms}^{-1}$ , for the six impingement angles.

impingement angle. As mentioned before, this may be an artefact of two-dimensional modelling.

#### 4.3.2 The investigation of the effect of precipitation rate on the ice accretion under varying impinging raindrop angle

The influence of precipitation rate on the ice accretion with various impingement angles has also been simulated. Two impingement angles,  $20^\circ$  and  $70^\circ$ , have been used. In Figure (4.9), the characteristic masses of the ice accretion and the accretion length are shown. The following values have been maintained constant: the external convective heat flux is  $150 \text{ Wm}^{-2}$ , the drop temperature is  $2^\circ\text{C}$ , and the simulation time is 5h.

For an impingement angle of  $70^\circ$ , the total impinging water increases most rapidly with rainfall rate. When the rainfall rate is  $1 \text{ mmh}^{-1}$ , the external convective heat flux is large enough to freeze all the impinging liquid, and there is no dripping from the ice accretion. Sufficient liquid fluxes cause the accretion below the cylinder to grow. When the rainfall rate increases to  $2 \text{ mmh}^{-1}$ , the pendant accretion (icicle) below the cylinder reaches its maximum length, and there is dripping from the tip of the accretion. A further increase in the rainfall rate leads to a rapid decrease in the accretion length below the cylinder. The total accretion mass reaches its maximum when the rainfall rate is  $4 \text{ mmh}^{-1}$ . Thereafter the total accretion mass diminishes slowly. For a  $20^\circ$  impingement angle, the total impinging rainfall and total accretion mass increase at first with increasing rainfall rate. All the impinging water freezes until the rainfall rate reaches about  $5 \text{ mmh}^{-1}$ . Thereafter part of the

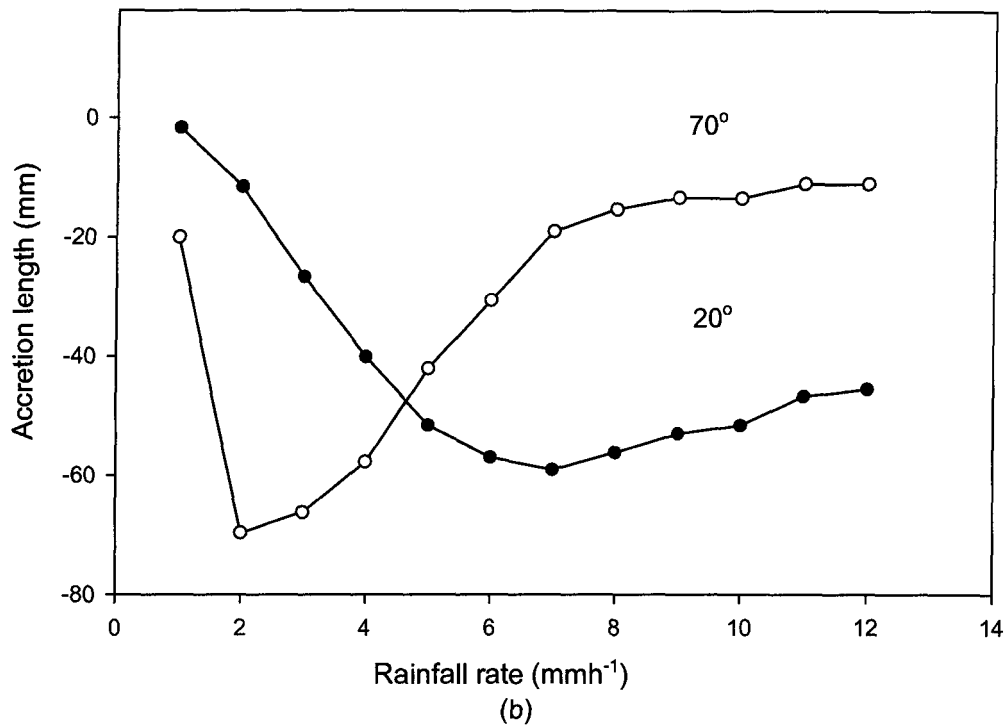
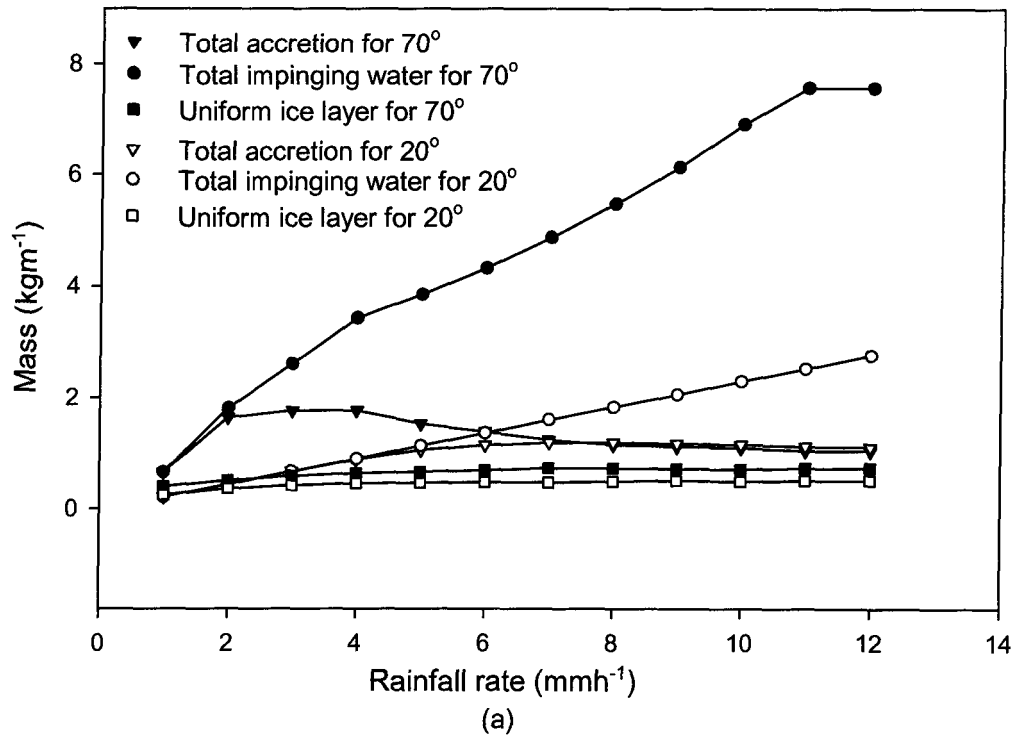


FIG. 4.9. The influence of rainfall rate on the ice accretion for two impingement angles, 20° and 70°. External convective heat flux is 150 Wm<sup>-2</sup>, drop temperature +2°C, simulation time 5h. (a) Variation of the characteristic masses. (b) Variation of the accretion length.

impinging water drips, but the total accretion mass continues to increase along with the total impinging water mass until they reach a maximum at a rainfall rate of  $7 \text{ mmh}^{-1}$ . At this point, the accretion length below the cylinder also reaches a maximum. A further increase in the rainfall rate causes the total accretion mass and the accretion length to decrease. It may be noticed in Figure (4.9) that when the rainfall rate is sufficiently high, a further increase in the rainfall rate doesn't change the total accretion mass for the two impingement angles, even though there is much more impinging water received by the accretion at the higher angle. In view of the uniform ice layer mass and accretion length shown in Figure (4.9), we can infer that more accretion is formed on the upwind side of the cylinder in the  $70^\circ$  case.

## CHAPTER 5

### SUMMARY AND RECOMMENDATIONS

#### 5.1 Summary

Numerical continuous models based on the assumption of continuous changes of all the physical parameters used in the prediction of ice accretion on wires have been reviewed. The principles of the random walk method developed by Szilder and Lozowski have also been reviewed. A two-dimensional random-walk model has been developed by the present author to simulate ice accretion due to freezing rain on a horizontal transmission line conductor. The shape and mass of the accretion growth have been predicted, including the effect of impinging droplet angle and the heating effect of the electric current.

Major assumptions made in the model include:

1. The conductor is placed horizontally; it is torsionally stiff and not subject to rotation.
2. In the simulation of ice accretion when considering the Joule heating effect, the electric current and the resistance of the conductor are assumed to be constant.
3. The wind is considered to be horizontal and perpendicular to the conductor in the simulation of the ice accretion under a variable raindrop impingement angle. For other cases, a calm wind is assumed.

The modelling results suggest that icicle formation is a strong function of the external convective heat flux. The icicle behaviour predicted by the random walk model is

in qualitative agreement with that predicted by the classical icicle growth model of Makkonen (1988), and with the experimental results of Maeno and Takahashi (1984), both of which show that after an icicle reaches a certain length, further increases in the liquid supply rate will make it shorter, rather than longer. When taking account of the Joule heating effect, a greater external convective heat flux is needed for the appearance of ice accretion on the conductor. The wind affects the impact angle of the impinging raindrops and the motion of the fluid elements, as well as the surface convective heat transfer. The simulations show that, for specified precipitation rate and atmospheric conditions, the total impinging rainfall increases with impinging raindrop angle. The total accretion mass increases first along with the raindrop impingement angle, then decreases. The maximum accretion mass occurs at a raindrop impingement angle around  $55^\circ$ . The icicle length exhibits a similar behaviour. When considering rainfall rate, the simulation shows that the ice accretion, under large raindrop impingement angles reaches the maximum mass and length at lower rainfall rates. When the rainfall rate is sufficiently high, a further increase in the rainfall rate doesn't change the total accretion mass significantly, even though there is much more impinging water received by the accretion with large raindrop impingement angles.

## 2. Recommendations

There are three main recommendations for the further work: 1) When the current model is used to simulate ice accretion with the Joule heating effect, an energy balance equation appropriate for the initial stages of the accretion was used in the deduction of the

model parameters for the entire accretion process. A relation between this equation and the accretion development should be established. In particular, one needs to take into account the Joule heating effect on the inner surface of the ice accretion. 2) For the simulation of ice accretion under the varying impinging raindrop angles, the limitation of the current two-dimensional model prevents the precise simulation of the shape of the icicle. Proceeding to a three-dimensional model is essential. 3) Ways to relate the microscopic model parameters to the macroscopic environmental parameters also need to be improved based on controlled physical experiments in a wind tunnel.

A series of cold room experiments will be undertaken in the new laboratory located at the Université du Québec à Chicoutimi. A 35mm diameter ACSR (aluminum conductor steel reinforced) “Bersimis” transmission line conductor will be used in the experiments. Water droplets sprayed by a set of nozzles mounted above the conductor will be used to simulate the precipitation. The spray rate and droplet size can be controlled by changing the water supply rate and the air pressure supplied to the nozzles. The refrigerator in the cold room can set the room temperature to a suitable range to simulate the atmospheric environment in freezing rain. A cold air stream produced by an electric fan mounted in the refrigerator will be used to simulate the wind. The electric voltage and current inside the conductor transmission line will also be controlled.

Due to the time limitation of this stage of the research, all the work mentioned above will be carried out in the next doctoral stage of the work.

## REFERENCES

- [1] Baker, P. G., G. Poots and G. G. Rodgers, 1986. Ice Accretion on Cables of Various Cross-Sections. *IMA J. Appl. Math.*, 36(1), 11-28.
- [2] Best, AC, (1949). "The Size Distribution of Raindrops," *Quart. J. Roy. Meteor. Soc.*, 76, pp. 16-36.
- [3] Chaîné PM and Castonguay G (1974) "New Approach to Radial Ice Thickness Concept Applied to Bundle-Like Conductors," Industrial Meteorology-Study IV, Environment Canada, Toronto, 11 pp.
- [4] Chung, KK and Lozowski, EP (1990). "On the Growth of Marine Icicles," *Atmosphere-Ocean*, Vol 28, No 4, pp. 393-408
- [5] Gunn, and G.D. Kinzer (1949). "The Terminal Velocity of Fall for Water Droplets in Stagnant Air," *J Meteor.*, Vol 6.
- [6] IEEE Power Engineering Society, (1993). "Standard for Calculating the Current-Temperature Relationship of Bare Overhead Conductors," IEEE Std 738-1993.
- [7] Jones, KF (1996), "A Simple Model for Freezing Rain Ice Loads," *Proc 7<sup>th</sup> International Workshop on Atmospheric Icing of Structures*, Chicoutimi, QC, pp. 412-416.
- [8] Lozowski, EP, Stallabrass, JR, and Hearty, PF (1983). "The Icing of an Unheated, Non-Rotating Cylinder. Part I: A Simulation Model," *J Clim. Appl. Meteorol.*, Vol 22, pp 2053-2062.

- [9] Maeno, N, and Takahashi, T (1984). "Studies on Icicles. I. General Aspects of the Structure and Growth of an Icicle," *Low Temp Sci Ser A*, Vol 43, No 6, pp. 125-138 (in Japanese).
- [10] Mason, BJ, (1971). "The Physics of Clouds ," Clarendon Press, Oxford, 2<sup>nd</sup> Ed, pp. 610.
- [11] Makkonen, L, (1984). "Modelling of Ice Accretion on Wires," *J Clim. Appl. Meteorol.*, Vol 23, No 6, pp. 929-939.
- [12] Makkonen, L, (1988). "The Growth of Icicles," *Proc 4<sup>th</sup> International Workshop on Atmospheric Icing of Structures*, pp. 236-242
- [13] Makkonen, L, and Fujii, Y (1993). "Spacing of Icicles," *Cold Reg. Sci. Technol.*, Vol 21, No 3, pp. 317-322.
- [14] Makkonen, L, (1996). "Modelling Power Line Icing in Freezing Precipitation" *Proc 7<sup>th</sup> International Workshop on Atmospheric Icing of Structures*, Chicoutimi, QC, pp. 195-200.
- [15] McComber, P. (2000). "A Non-Circular Accretion Shape Freezing Rain Model for Transmission Line Icing," *Proc 9<sup>th</sup> International Workshop on Atmospheric Icing of Structures*, Chester, England.
- [16] Nikiforov, YuP, (1982). "Icing Related Problems, Effect of Line Design and Ice Mapping," *Special Rep.* 83-17, U.S. Army Cold Regions Res. Eng. Lab., Hanover, NH, pp. 239-245.
- [17] Stallabrass, JR, (1983). "Aspects of Freezing Rain Simulation and Testing," *Proc 1<sup>st</sup> International Workshop on Atmospheric Icing of Structures*, Hanover, NH, pp. 67-74.

- [18] Stallabrass, JR and Hearty, PF (1967). "The Icing of Cylinders in Conditions of Simulated Freezing Sea Spray," *DME Report MD-50*, National Research Council of Canada, 15 pp.
- [19] Szilder, K. (1993). "The Density and Structure of Ice Accretion Predicted by a Random-Walk Model," *Quart. J. Roy. Meteor. Soc.*, Vol 119, No 513, pp. 907-924.
- [20] Szilder, K. (1994). "Simulation of Ice Accretion on a Cylinder Due to Freezing Rain," *J Glaciol*, Vol 40, No 136, pp586-594.
- [21] Szilder, K, and Lozowski, EP (1995a). "A New Method of Modelling Ice Accretion on Objects of Complex Geometry," *Int. J Offshore Polar Engng. Conf., ISOPE*, Vol 5, No 1, pp. 34-42.
- [22] Szilder, K, and Lozowski, EP (1995b). "Simulation of Icicle Growth Using a Three-Dimensional Random Walk Model," *Atmospheric Research*, Vol 36, No 1, pp. 243-249.
- [23] Szilder, K, Forest, TW, and Lozowski, EP (1995c). "Experimental Verification of a Pendant Ice Formation Model," *Proc. 5<sup>th</sup> Int. Offshore Polar Engng. Conf., ISOPE*, The Hague, Vol II, pp. 469-475.
- [24] Szilder, K, and Lozowski, EP (1999). "Morphogenetic Modelling of Wet Ice Accretions on Transmission Lines as a Result of Freezing Rain," *Proc. 9<sup>th</sup> Int. Offshore Polar Engng. Conf., ISOPE*, Brest, Vol II, pp. 616-621.
- [25] Tan, H and Tian, S (1990). "Fortran language," Tsinghua Univ. Publishing House.

## Appendix A

```

*****
*           The FORTRAN program of Makkonen's numerical model           *
*****

```

```

PROGRAM MAIN
IMPLICIT NONE

```

```

*****
* Definition of the variables                                           *
* AT, accretion duration; d, droplet diameter; D0, the bare cylinder   *
* diameter; Dc, the cylinder diameter in the each step of calculation; *
* DeltaT, time step; Dn, the cylinder diameter calculated in the      *
* each step; E, cylinder collection efficiency calculated as a        *
* fractional sum of the collection efficiencies for each droplet      *
* size category; EK0, name of the function; Em, collection            *
* efficiency calculated using the median volume droplet; h, heat      *
* transfer coefficient; I, icing intensity; K0, parameter to calculate *
* E; M, ice load; Mn, ice load in each step; n, freezing fraction;    *
* PI,  $\pi$ ; R, Mackin's density parameter; RO, ice density;      *
* ta, air temperature; TRO, total deposit density; v, wind velocity;  *
* w, liquid water content; Y, counter.                                  *
*****

```

```

DOUBLE PRECISION AT, d, D0, Dc, DeltaT, Dn, E, Em, h, I, K0, M,
DOUBLE PRECISION Mn, N, PI, Pa, R, RO, ta, TRO, ts, v, w, Y
PARAMETER (PI=3.1415926D0)

```

```

WRITE(*,*)'PLEASE INPUT THE AIR TEMPERATURE:'
READ*,ta
WRITE(*,*)'PLEASE INPUT THE WINDSPEED:'
READ*,v
WRITE(*,*)'PLEASE INPUT THE WATER CONTENT:'
READ*,w
WRITE(*,*)'PLEASE INPUT THE DROPLET DIAMETER:'
READ*,d

```

```

WRITE(*,*)'PLEASE INPUT THE CYLINDER DIAMETER:'
READ*,Dn
WRITE(*,*)'PLEASE INPUT THE AIR PRESSURE:'
READ*,Pa
WRITE(*,*)'PLEASE INPUT THE ACCRETION DURATION:'
READ*,AT
WRITE(*,*)'PLEASE INPUT THE TIME STEP:'
READ*,DeltaT

Mn=0.0D0
D0=Dn

OPEN(UNIT=2, FILE="RESULT")

DO 100,Y=0,AT,DeltaT
  M=Mn
  Dc=Dn
  K0=EK0(v,d,Dc,ta,Pa)
  CALL EEM(K0,Em)
  CALL EQU(Em,E)
  h=EH(v,Dc,ta,Pa)
  CALL En(E,v,w,ta,Dc,h,Pa,n)
  CALL ETS(E,v,w,ta,h,Pa,ts)
  CALL ER(K0,d,ts,v,R)
  CALL ERO(R,RO)
  I=n*E*v*w/PI
  Mn=M+I*PI*Dc*DeltaT*36.0D2
  Dn=(4.0*(Mn-M)/(PI*RO)+Dc**2)**(1.0/2.0)
  TRO=4.0*Mn*(PI*Dn**2-PI*D0**2)**-1
  WRITE(2,200) Y, Dc*1.0D2, I*2.0d4, RO, M, TRO, n, E
10  FORMAT(1x,f8.2, 2x, f8.4, 2x, f8.4, 2x,f8.4, 2x,f8.4, 2x,
& f8.4,2x, f8.4,2x, f8.4,2x, f8.4)
10  CONTINUE

CLOSE(unit = 2)

```

STOP  
END

```
*****  
*           Function to calculate the parameter K0           *  
*****
```

```
DOUBLE PRECISION FUNCTION EK0(v,d,Dc,ta,Pa)  
IMPLICIT NONE  
DOUBLE PRECISION Row, X, Roa, K, Red, v, Dc, d, ta, MU,  
& a,b,MU0,Pa  
Row=1.0D3  
X=MU(ta)  
mu0=1.8325D-5  
Roa=Pa/(287.05*(ta+273.15))  
K=(Row*v*d**2.0)/(9.0*x*Dc)  
Red=Roa*d*v/x  
EK0=K*(0.087*Red**(0.76*Red**-0.027)+1)**-1  
RETURN  
END
```

```
*****  
*           Function to calculate the absolute viscosity of air           *  
*           as a function of temperature                               *  
*****
```

```
DOUBLE PRECISION FUNCTION MU(T)  
IMPLICIT NONE  
DOUBLE PRECISION MU0,t0,C,T  
MU0=1.8325D-5  
t0 = 296.16D0  
C = 120.0D0  
MU=MU0*((t0+C)/(T+273.15+C))*((T+273.15)/t0)**(3.0/2.0)  
RETURN
```

END

```
*****
*           Subroutine to calculate collection efficiency           *
*           calculated using the median volume droplet Em         *
*****
```

```
      SUBROUTINE EEM(K,Em)
      IMPLICIT NONE
      DOUBLE PRECISION Em, K, ESE, EGE
      IF (K.GT.0.8) THEN
      Em = K**1.1*(K**1.1+1.426)**-1
      ELSE
      Em = 0.5*(DLOG10(8.0*K))**1.6
      END IF
      RETURN
      END
```

```
*****
*           Subroutine to calculate collection efficiency E with Em *
*****
```

```
      SUBROUTINE EQU(Em,E)
      DOUBLE PRECISION Em,E
      E=0.69*EM**0.67+0.31*EM**1.67
      END
```

```
*****
*           Function to calculate convective heat transfer coefficient h *
*****
```

```
      DOUBLE PRECISION FUNCTION EH(v,Dc,ta,Pa)
      DOUBLE PRECISION v,Dc,ta,Ka,Roa,a,x,mu,Pa
```

```

Roa=Pa/(287.05*(ta+273.15))
Ka=2.53D-2
X=MU(ta)
EH=Ka*0.032*(Roa*Dc*v/X)**0.85/Dc
END

```

```

*****
*           Subroutine to calculate the freezing fraction n           *
*****

```

```

SUBROUTINE En(E,v,w,ta,Dc,h,Pa,n)
IMPLICIT NONE
DOUBLE PRECISION PI,SBC,Cw,Ci,k,Le,a,Lf,Cp,Pa,r,t1,t2,
& w,h,ea,Dc,n, e0,ts,ta,E,v,c,b,x,y,z
PI=3.1415926D0
Lf=0.3337D6
k=0.62D0
Le=2.5008D6
Cp=1005D0
r=0.79D0
Cw=4218D0
SBC=5.6697D-8
a=8.1D7
CALL EVP(0.0,e0)
CALL EVP(ta,ea)
n=PI*h*(-ta+k*Le*(e0-ea)/(Cp*Pa)-r*v**2.0/(2.0*Cp))/
& (2.0*E*v*w*Lf)-ta/Lf*(Cw+PI*SBC*a/(2.0*E*v*w))
IF (n.GT.1) THEN
n=1
END IF
RETURN
END

```

```
*****
*      Subroutine to calculate the saturation water vapour pressure      *
*****
```

```

SUBROUTINE EVP(T,E)
DOUBLE PRECISION T,E
E=0.6112*DEXP(17.67*T/(T+243.5))*1.0D3
RETURN
END
```

```
*****
*      Subroutine to calculate the ice accretion surface temperature ts  *
*****
```

```

SUBROUTINE ETS(E,v,w,ta,h,Pa,ts)
IMPLICIT NONE
DOUBLE PRECISION F,F1,F2,PI,SBC,Lf,Cw,Ci,k,Ls,Cp,Pa,r,
& E,v,w,h,ea,t1,t2,ts,ta,a,EF,t
EF(t)=2*E*v*w*(Lf + Cw*ta - Ci*t)/PI - h*((t - ta)
& +k*Ls*(0.6112*DEXP(17.67*t/(t+243.5))*1.0D3-ea)/
& (Cp*Pa) -r*v**2/(2*Cp)) -SBC*a*(t-ta)
PI=3.1415926D0
SBC=5.6697D-8
Lf=0.3337D6
Cw=4218D0
Ci=2106D0
k=0.62D0
Ls=2.8366D6
Cp=1005D0
r=0.79D0
a=8.1D7
CALL EVP(ta,ea)
t1=-40.0D0
t2=10.0D0
```

```

F1=EF(t1)
F2=EF(t2)
10  ts = (t1 + t2)/2.0
F=EF(ts)
IF (SIGN(F,F1).EQ.F) THEN
  t1=ts
  F1=F
END IF
IF (SIGN(F,F2).EQ.F) THEN
  t2=ts
  F2=F
END IF
IF ((ABS(t1-t2).GT.1D-10).OR.(F.GT.1D-12)) GOTO 10
IF (F.GT.1D-12) ts=(t1+t2)/2.0
RETURN
END

```

```

*****
*           Subroutine to calculate Macklin's density parameter      *
*****

```

```

SUBROUTINE ER(K0, dm, ts, v, R)
IMPLICIT NONE
DOUBLE PRECISION K0, R, dm, ts, v, v0
IF (K0.LE.0.55) THEN
  v0=v*(-0.174+1.464*K0-0.816*K0**2)
ELSE
  v0=v*(0.561+0.592*DLOG10(K0)-0.26*(DLOG10(K0))**2)
END IF
IF ((ts.gt.0.0d0).or.(abs(ts).lt.1.0D-8)) THEN
  R=70.0D0
ELSE
  R=-v0*dm*1.0D6/(2.0*ts)
END IF

```

```
RETURN
END
```

```
*****
*                               Subroutine to calculate ice density  $\rho$                                *
*****
```

```
      SUBROUTINE ERO(R,RO)
      DOUBLE PRECISION R,RO
      IF (R.LT.0.9) THEN
        RO = 100D0
      ELSE IF (R.LE.10.0) THEN
        RO = 0.11 * R**0.76*1.0D3
      ELSE IF (R.LE.60.0) THEN
        RO=(R*(R+5.61)**-1)*1.0D3
      ELSE
        RO=0.92D3
      ENDIF
      RETURN
      END
```

## **Appendix B**

```
*****
*                               The FORTRAN program of Lozowski's model                               *
*****
```

```
PROGRAM MAIN
IMPLICIT NONE
INTEGER I, J
```

```
*****
* Definition of the variables: *
* B, array to calculate the overall collision efficiency; Beta, array *
* to calculate the Collision efficiency for different angles; Cita, *
* the angles of divided upwind face of the cylinder; D, the droplet *
* diameter; Dc, the diameter of the cylinder; DeltaT, accretion time *
* step; E, the collection efficiency; EB, fonction to calculate the *
* collision efficiency; h, heat transfer coefficient; Pa, air pressure; *
* PI,  $\pi$ ; n, freezing fraction; R, icing flux; Roi, the density of the *
* ice; Rw, droplet mass flux; Rws, runback mass flux; ta, air *
* temperature; th, ice accretion thickness; ts, runback water *
* temperature; U, wind velocity; w, liquid water content; z, temporary *
* variable as 0. *
*****
```

```
DOUBLE PRECISION B(0:18,1:9),Beta(0:18),Cita(0:18),D(1:9),Dc,
&DeltaT,E,EB,h,Pa,PI,n(0:18),R(0:18),ROi,Rw(0:18),Rws(0:18),
&ta,th(0:18),ts(0:18),U,w,z
```

```
PARAMETER (PI = 3.1415926D0)
```

```
*****
*                               Input the parameters                               *
*****
```

```
PRINT*, 'ENTER AIR TEMPERATURN (C), ta = '
```

```

READ(*,*) ta
PRINT*, 'ENTER WIND SPEED (m/s), U = '
READ(*,*) U
PRINT*, 'ENTER LIQUID WATER CONTENT (kg/m3), w = '
READ(*,*) w
PRINT*, 'ENTER AIR PRESSURE (Pa), Pa = '
READ(*,*) Pa
PRINT*, 'ENTER ACCRETION TIMESTEP (s), DeltaT = '
READ(*,*) DeltaT
Dc = 2.54D-2
ROi = 890.0D0

```

```

*****
*           The main calculation to get the thickness           *
*           of the accretion for each angular sector           *
*****

```

```

DO 100 I = 0,18
  CITA(I) = 5.0*I
  DO 200 J = 1,9
    D(J) = 5.0*J*1.0D-6
    B(I,J) = EB(U,Dc,Pa,ta,D,Cita,I,J)
200 CONTINUE
  Beta(I) = 0.06*B(I,1)+0.10*B(I,2)+0.19*B(I,3)+0.29*B(I,4)+
& 0.18*B(I,5)+0.08*B(I,6)+0.05*B(I,7)+0.035*B(I,8)+0.015*B(I,9)
  Rw(I) = Beta(I)*U*w
  Rws(I) = 0.0d0
  IF (I.EQ.1) Rws(I) = (1-n(I-1))*(Rw(I-1)+0.5*Rws(I-1))
  IF (I.GE.2) Rws(I) = (1-n(I-1))*(Rw(I-1)+Rws(I-1))
  z = 0.0
  IF (I.GE.1) THEN
    CALL ENT(U,w,ta,Pa,Rw(I),Cita(I),Rws(I),ts(I-1),Dc,n(I),ts(I))
  ELSE
    CALL ENT(U,w,ta,Pa,Rw(I),Cita(I),Rws(I),z,Dc,n(I),ts(I))
  END IF

```

```

      R(I) = n(I)*(Rw(I)+Rws(I))
      th(I) = (2.0*R(I)*DeltaT/ROi)/(1.0+(1.0+4.0*R(I)*DeltaT/
& (ROi*Dc)**0.5)
100  CONTINUE

```

```

*****
*                               Output the results                               *
*****

```

```

      OPEN (unit = 1, file = "Thickness")
      DO I = 0,18
      WRITE(1,300) th(I)
300  FORMAT(1x,E12.6)
      ENDDO
      CLOSE(unit = 1)
      STOP
      END

```

```

*****
*                               The function to calculate the collision efficiency   *
*****

```

```

      DOUBLE PRECISION FUNCTION EB(U,Dc,Pa,ta,D,Cita,I,J)
      IMPLICIT NONE
      DOUBLE PRECISION ROW, X, ROa,Pa,K, Rej, U, Dc, ta, MU,
&PI,BETA0,k0,E,CITAM,CITA(0:18),B(0:18,1:9),D(1:9),MUa
      INTEGER I,J
      PI = 3.1415926
      ROW = 1.0D3
      MUa = MU(ta)
      ROa = Pa/(287.05*(ta+273.15))
      Rej = D(J)*U*ROa/MUa
      K = (ROW*U*D(J)**2.0)/(9.0*MUa*Dc)
      K0 = 0.125+(K-0.125)/(1.0+0.0967*Rej**0.6367)

```

```

IF (K0.LT.0.125) THEN
  BETA0 = 0.0
  E = 0.0
  CITAM = 0.0
END IF
IF ((K0.GE.0.125).AND.(K0.LE.7.5)) THEN
  BETA0 = 1.4*(K0-0.125)**0.84/(1+1.4*(K0-0.125)**0.84)
ELSE IF (K0.GE.7.5) THEN
  BETA0 = K0/(1+K0)
END IF
IF ((K0.GE.0.125).AND.(K0.LT.0.9)) THEN
  E = 0.489*(DLOG10(8.0*K0))**1.978
ELSE IF (K0.GE.0.9) THEN
  E = K0/(PI/2.0+K0)
END IF
IF ((K0.GE.0.125).AND.(K0.LE.10.0)) THEN
  CITAM = (ATAN(1.7*(K0-0.125)**0.76))*180.0/PI
ELSE IF (K0.GE.10.0) THEN
  CITAM = (ATAN(K0))*180.0/PI
END IF
IF (CITA(I).LT.CITAM) THEN
  EB = BETA0*COS(CITA(I)/CITAM*PI/2.0)+PI**3.0/
& ((CITAM*PI/180.0)**3*(PI**2-4.0))*(E-2.0*CITAM*BETA0/180.0)*
& (CITA(I)*PI/180.0)**2*SIN(CITA(I)/CITAM*PI)
ELSE
  EB = 0.0
END IF
RETURN
END

```

```

*****
*           Function to calculate the absolute viscosity of air           *
*           as a function of temperature                                 *
*****

```

```

DOUBLE PRECISION FUNCTION MU(T)
IMPLICIT NONE
DOUBLE PRECISION MU0,t0,C,T
MU0 = 1.8325D-5
t0 = 296.16D0
C = 120.0D0
MU = MU0*((t0+C)/(T+273.15+C))*((T+273.15)/t0)**(3.0/2.0)
RETURN
END

```

```

*****
*           The subroutine to calculate the saturation vapour pressure    *
*           as a function of different temperature                       *
*****

```

```

SUBROUTINE EVP(T,E)
DOUBLE PRECISION T,E
E = 611.2*DEXP(17.67*T/(T+243.5))
RETURN
END

```

```

*****
*           The function to calculate the heat transfer coefficient      *
*****

```

```

DOUBLE PRECISION FUNCTION Eh(Cita,U,ta,Dc,Pa)
IMPLICIT NONE
DOUBLE PRECISION Dc,Ka,Nu,Cita,Rec,X,ROa,K,U,ta,MU,PI,Pa,MUa
PI = 3.1415926

```

```

Ka = 2.53D-2
MUa = MU(ta)
ROa = Pa/(287.05*(ta+273.15))
Rec = U*Dc*ROa/MUa
Nu = Rec**(0.5)*(2.4+1.2*SIN(3.6*(Cita*PI/180.0-0.44)))
Eh = Ka*Nu/Dc
RETURN
END

```

```

*****
*           The subroutine to calculate the freezing fraction or           *
*           the runback water temperature                               *
*****

```

```

SUBROUTINE ENT(U,w,ta,Pa,Rw,Cita,Rws,tss,Dc,n,ts)
IMPLICIT NONE
DOUBLE PRECISION h,ta,ts,ea,es,e0,lv,cp,epsilon,Cita,
&Rw,Rws,n,tss,f,lfs,Pr,Sc,rc,cw,n1,n2,t1,t2,f1,f2,Eh,Et,E,
&E1,E2,Dc,U,En,t,w,Pa,PI
EN(n) = h*ta+h*(Pr/Sc)**0.63*lv*epsilon/(Pa*cp)*(ea-e0)+
&h*rc*U**2.0/(2.0*cp)+0.5*Rw*U**2+Rw*lfs*n+Rw*cw*ta+
&Rws*cw*tss+Rws*lfs*n
ET(t) = h*(ta-t)+h*(Pr/Sc)**0.63*lv*epsilon/(Pa*cp)*(ea-
&611.2*DEXP(17.67*t/(t+243.5)))+h*rc*U**2.0/(2.0*cp)+
&0.5*Rw*U**2.0+Rw*lfs+Rw*cw*(ta-t)
&+Rws*cw*(tss-t)+Rws*lfs
CALL EVP(ta,ea)
h = Eh(Cita,U,ta,Dc,Pa)
e0 = 611.2D0
cp = 1005.0D0
cw = 4.27D3
lfs = 3.337D5
lv = 2.5008D6
epsilon = 0.622D0
PI = 3.1415926D0

```

```

Pr = 0.711D0
Sc = 0.595D0
rc = 0.75+0.25*COS(2.0*(Cita*PI/180.0))
n1 = -10.0D0
n2 = 15.0D0
F1 = En(n1)
F2 = En(n2)
10  n = (n1+n2)/2.0
    F = En(n)
    IF (SIGN(F,F1).EQ.F) THEN
        n1 = n
        F1 = F
    END IF
    IF (SIGN(F,F2).EQ.F) THEN
        n2 = n
        F2 = F
    END IF
    IF ((ABS(n1-n2).GT.1.0D-10).OR.(F.GT.1.0D-12)) GOTO 10
    IF (F.GT.1.0D-12) n = (n1+n2)/2.0
    IF (n.GT.1.0) THEN
        n = 1.0d0
        t1 = -40.0D0
        t2 = 10.0D0
        E1 = Et(t1)
        E2 = Et(t2)
20  ts = (t1+t2)/2.0
    E = Et(ts)
    IF (SIGN(E,E1).EQ.E) THEN
        t1 = ts
        E1 = E
    END IF
    IF (SIGN(E,E2).EQ.E) THEN
        t2 = ts
        E2 = E
    END IF
    IF ((ABS(t1-t2).GT.1.0D-10).OR.(E.GT.1.0D-12)) GOTO 20

```

```
IF (E.GT.1.0D-12) ts = (t1+t2)/2.0  
END IF  
RETURN  
END
```